Syngas Production, Storage, Compression and Use in Gas Turbines

Minjiao Yang [1]

Haiping Yang [1,2]

Hewen Zhou [1]

Qing Yang [1]

Haibo Zhao [2]

Eid Gul [1]

Mohsin Ali Khan [3]

Oyvind Skreiberg [4]

Liang Wang [4]

He Chao [5]

Pietro Bartocci [6]✉

Email bartocci@crbnet.it

Katarzyna Slopiecka [6]

Gianni Bidini [6]

Francesco Fantozzi [6]

[1] China-EU Institute for Clean and Renewable Energy, Huazhong University of Science and Technology, Wuhan, Hubei, China

[2] State Key Laboratory of Coal Combustion, Huazhong University of Science and Technology, Wuhan, Hubei, China

[3] University of Haripur Pakistan, Haripur, KPK, Pakistan

[4] SINTEF Energy Research, Trondheim, Norway

[5] School of Chemical and Biomedical Engineering, Nanyang Technological University, Singapore, Singapore

[6] Department of Engineering, University of Perugia, Perugia, Italy

Abstract

This chapters analyses syngas production through pyrolysis and gasification, its compression and its use in gas turbines. Syngas compression can be performed during or after thermal treatment processes. Important points are discussed related to syngas ignition, syngas explosion limit at high temperatures and high pressures and syngas combustion kinetics. Kinetic aspects influence ignition and final emissions which are obtained at the completion of the combustion process. The chapter is organised into four subsections, dealing with (1) innovative syngas production plants, (2) syngas compressors and compression process, (3) syngas ignition in both heterogeneous and homogeneous systems and (4) syngas combustion kinetics and experimental methods. Particular attention is given to ignition regions that affect the kinetics, namely systems that operate at temperatures higher than 1000 K can have strong ignition, whereas those operating at lower temperatures have weak ignition.
AQ1

Keywords

Pyrogas
Pyrolysis
Ignition
Syngas
Compression
Gasification

12.1. Innovative Pyrolysis and Gasification Plants

Seven pyrolysis plants are discussed herein: (1) integrated pyrolysis regenerated plant (IPRP), (2) pyrolysis polygeneration plant, (3) Carbofex plant, (4) Carbon Terra plant, (5) Pyreg plant, (6) TCR® plant and (7) 3R Agrocarbon plant. Each of these plants and their developing organisations is described briefly next. The IPRP design was developed by the University of Perugia (Italy) with collaboration of BIONET-Biomass and New Technologies and Biomass Research Centre, University of Perugia and it is now located in the Terni site. The IPRP pilot is based on a rotary kiln pyrolysis reactor. The pyrolysis polygeneration plant was developed by the State Key Laboratoy on Coal Combustion (SKLCC) of Huazhong University of Science and Technology (HUST) and is basd on a moving bed reactor. The Carbofex plant was developed by a Finnish company producing charcoal to be used as fertilizer and filter. The Carbofex reactor is based on an auger reactor. The Carbon Terra plant was developed by a German company, named Carbon Terra which has developed the Schottdorf-Meiler kiln. The Pyreg plant was developed by a German company named Pyreg which has developed a reactor heated at (500–700) °C and in which biomass is moved by screw conveyors. The thermo-catalytic reforming (TCR) plant was developed by a German company (Susteen) who commercialized the TCR® plant for pyrolysis that is coupled to reforming. The 3R Agrocarbon plant was developed by Terra Humana company; the technology is called 3R Agrocarbon. The 3R Agrocarbon plant is based on a rotary kiln reactor.
AQ2

Together with the seven pyrolysis plants, three gasification plants are presented: (1) Milena (developed at ECN – now TSO – in the Netherlands), (2) Güssing gasifier, developed by a consortium

called “Renet Austria” with important participation of Technical University of Vienna and (3) GoBiGas, which was built in Gothenburg (Sweden) with the support of Chalmers university.

12.1.1. IPRP Technology

The integrated pyrolysis regenerated plant (IPRP), is an innovative technology which combines the rotary kiln pyrolyzer with a gas turbines (GTs) to make fully use of the pyrogas produced from biomass and waste thermal conversion.

The IPRP approach was proposed by D’Alessandro et al. [1]. The target of this project is to design a technology which can use the biomass with a higher efficiency. This technology mainly includes a GT fueled with syngas. The exhaust gases produced from the GT can be used to provide the energy required by the pyrolysis reactor. Figure 12.1 shows the exact layout of IPRP technology. The final outputs of the IPRP plant are represented by heat and electricity.

Fig. 12.1

Integrated pyrolysis regenerated plant (IPRP) concept. Reprinted with permission from [1] Copyright © 2013, Elsevier

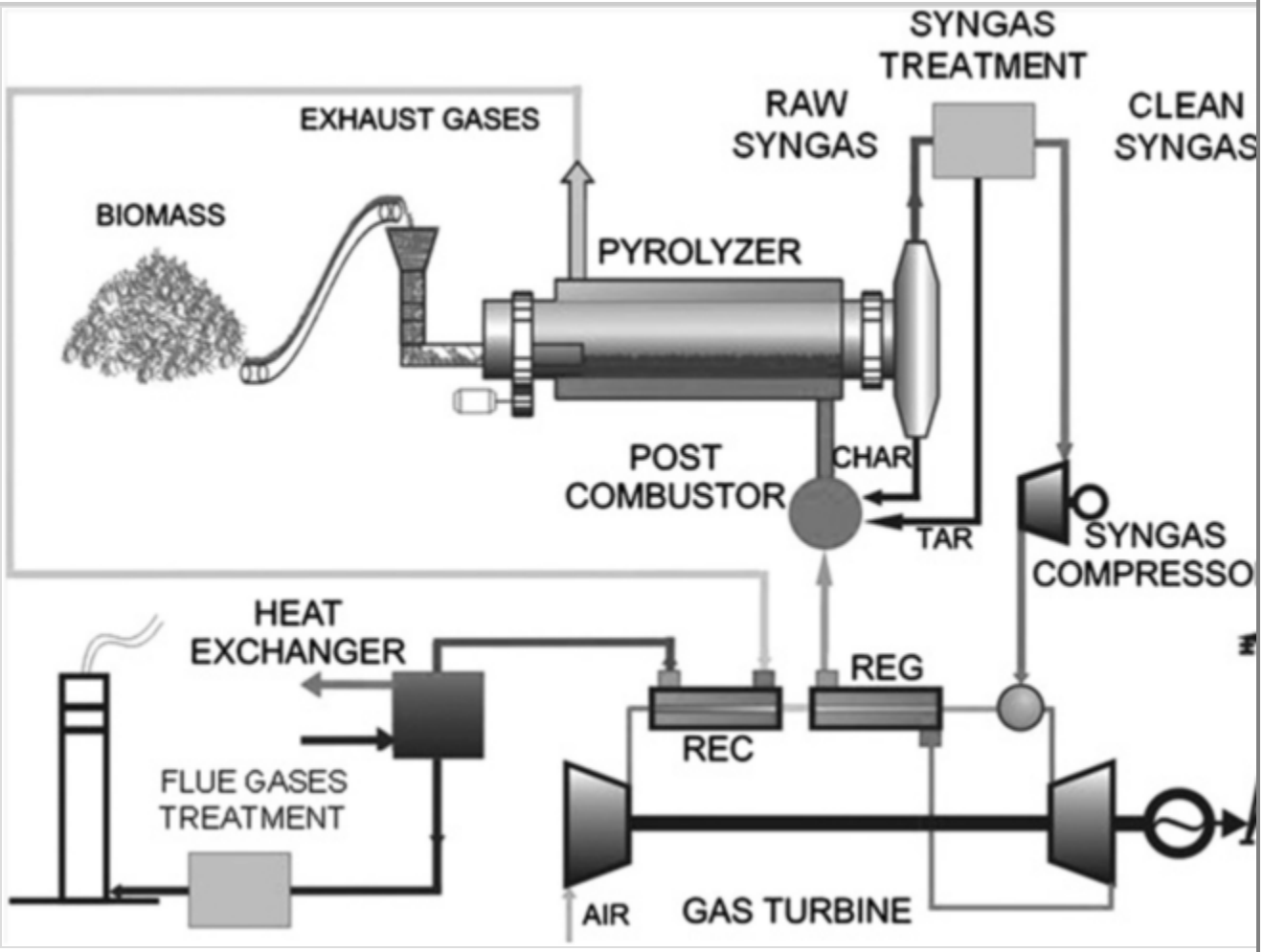

The heat is produced after two heat recovery stages (REG and REC) aiming at the full use of energy through the regeneration of exhaust heat by two-stage air preheating. There is one regenerator (REG) used to recover the thermal energy of exhaust gases out from the turbine, and one recuperator (REC) to recover the thermal energy of exhaust gases out from the pyrolysis reactor. A picture of the plant is shown in Fig. 12.2.

Fig. 12.2

Integrated pyrolysis regenerated plant (IPRP) demonstrative unit. Reprinted with permission from [1] Copyright © 2013, Elsevier

The feedstock is fed through a hopper into a rotary kiln pyrolyzer, which is made by a reaction chamber that thermally degrades into syngas, coke and tar in the absence of oxygen. The hermetic seal between the rotary kiln and the oven is achieved by a high temperature resistant graphite ring, while the hermetic seal between the rotary kiln and the inlet and outlet sections is achieved by a soft iron ring. The refractory chamber containing the pyrolysis furnace is equipped with a combustion system at the bottom which continuously feeds the char conveyed by the screw conveyor at the outlet portion of the pyrolysis furnace. Combusting char could provide the heat required for pyrolysis, the combustion air is provided by a dedicated blower or by the gas turbine exhaust gases. This depends on

operational requirements. Dual fuel gas burners exhaust gases (i.e. natural gas and syngas) are discharged directly into the refractory chamber above the char burner to provide the final additional heat for temperature control and startup. The particulates of syngas coming from the pyrolysis furnace are removed in a cyclone. Syngas finally is cooled to condense tar and water in the wet scrubbing section, which is comprised of a two-stage quencher for temperature reduction. This is made by a variable throat Venturi tube, consisting of a two-stage scrubber with a final demister. Heavy tar and light tar are extracted from the bottom and the top of the tank and can be returned to the dedicated burner in the refractory chamber of the pyrolysis furnace via a hot pipe, although this solution is still under investigation. The syngas is withdrawn from the pyrolysis furnace through the cleaning section by a side channel blower, and the speed of the side blower is adjusted to maintain a slight negative pressure in the rotary kiln, thereby providing the required pressure to the syngas compressor of the micro turbine. The micro turbine is coupled to a radial geometry turbo compressor with an annular combustion chamber suitable for combustion gases (the main parameters of the micro-turbine are shown in Table 12.1).

Table 12.1

Parameters of the micro gas turbine used in the IPRP demonstrative unit [1]

Parameter	Value
WE (kW)	80
μ_E (%)	27
Turbine inlet temperature (°C)	1010
Manometric compression ratio	4
Exhaust gases flow (kg/s)	0.77
Exhaust gases temperature (°C)	270
rpm	68,000

The compressor has an approximate compression ratio of 4. The radial turbine provides energy to drive compressors and alternators. Electrical energy is generated by a 4-pole permanent magn*et al*ternator that rotates within the oil-cooled stator assembly, which operates as an engine during initial startup, thereby reducing the need for auxiliary starting hardware. The micro turbine is equipped with a REG for preheating the combustion air by using the waste heat generated by the exhaust gas cooling; thereby reducing the exhaust gas temperature to approximately 270 °C.

12.1.2. Polygeneration Plant Based on Moving Bed in HUST

Given the abundance of agricultural residues in China, the biomass energy can play a significant role to satisfy at least part of the energy demand, granting environmental protection [2]. The thermal conversion technologies of biomass mainly involve combustion, gasification and pyrolysis. However, the combustion technology would release large amount of particulate matters with relative low energy efficiency [3]. In addition, biomass gasification has been widely used in China and there has been

over 70 gasification systems built. The heating value of syngas produced in applied air-gasification systems is still too lower to be used. Compared with these two technologies, the pyrolysis system converts biomass into three main products (i.e. pyrolysis gas, bio-oil and biochar), in which the heating value of pyrolysis gas is higher because no gasification medium is used in the reactor [4]. In addition, these high-quality products can bring economic benefits to the pyrolysis system. Thus, pyrolysis technology is an important and promising method for Chinese biomass utilization.

Particular interesting results the research and development of poly-generation pyrolysis systems to propmote the resource utilization of biomass. They have proposed a new poly-generation pyrolysis technology, and developed this technology to the commercial scale (see the demonstration poly-generation pyrolysis plant in Ezhou, Hubei Province, China). In addition, based on this moving-bed poly-pyrolysis technology, they have received the Blue Sky Award from the United Nations Industrial Development Organization in 2014. The layout of biomass polygeneration system demonstration plant is shown in Fig. 12.3.

Fig. 12.3

Biomass-based pyrolytic polygeneration demonstration system. Reprinted with permission from [2]. Copyright © 2018, Elsevier

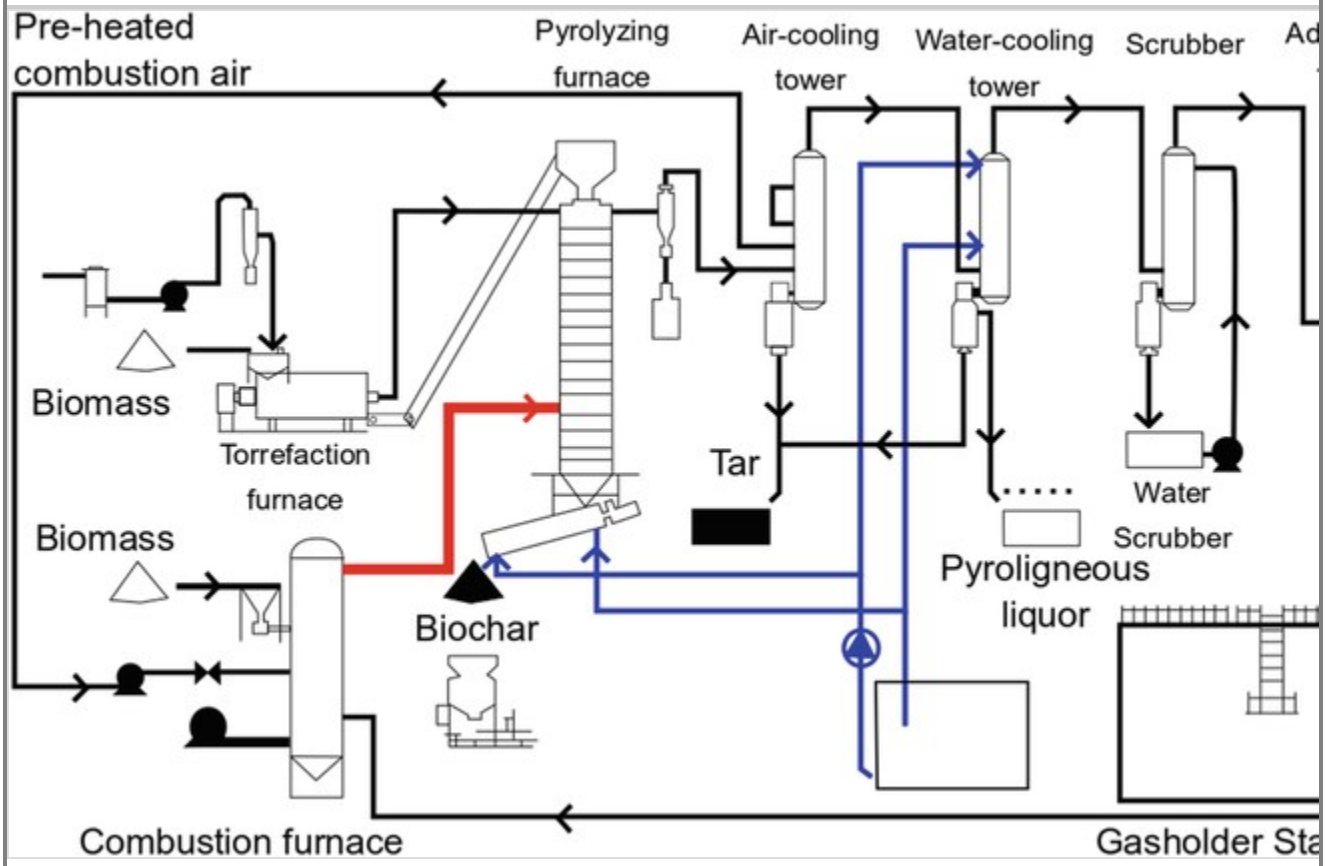

In Fig. 12.3, the biomass feedstock (e.g. agricultural residues and forest residues) would be firstly crushed to a particle size (<5 cm) and then sent to a torrefaction oven for 1 hour. The dried biomass pellets are fed from the top to the pyrolysis furnace (designed as moving bed) by high temperature.

Both the baking furnace and the pyrolysis furnace are in a closed atmosphere. In the moving bed pyrolysis furnace, the biomass particles move up and down under the action of gravity to complete the pyrolysis, and control the discharge time and quantity of the biochar, so that the biomass particle volatiles are completely released. The high temperature volatiles from the top of the pyrolysis furnace are sequentially passed to air cooling, water cooling, cleaning and adsorption towers to bring the temperature down to the range (40 °C–60 °C) to obtain liquid products (tar and vinegar) and purify the gas product (pyrolysis gas). Throughout the baking and pyrolysis process, heat is provided by the high temperature flue gas of the biomass burner. In order to increase the thermal efficiency of the system, the air required is from the heat exchanger of the air cooling tower. The calcining pyrolysis furnace can process 6 tons of biomass per hour (water content <20 wt%), and the furnace requires about 0.6 tons of biomass per hour. The temperature of the pyrolysis zone in the operating state of the pyrolysis cogeneration system is 600 °C.

12.1.3. Pyrolysis Plant at Carbofex

Carbofex is a technology developed in Finland. The plant is fed with (400–500) kg/h of dried wood chips and produces (100–140) kg of charcoal and (90–100) L of high quality pyrolysis oils. The syngas is in part burned to provide the heat required by the pyrolysis process and in part burned to provide heat to a district heating network. When in the summer heat is not required, an important part of the syngas can be stored, see [5].

12.1.4. Pyrolysis Plant at Carbon Terra

Carbon Terra pyrolysis plant is based on a reactor named Schottdorf kiln. The reactor is fed with 1 MW input of biomass [6, 7]. The power output for the products is composed by: 300 kW pyrolysis gas and 600 kW biochar (i.e. about 600 tons per year). The energy efficiency is between (90 to 95) %. The operating temperature of the process is about (800–900) °C. During the start-up phase, it dry biomass is used. The char outlet is at the bottom of the reactor. Char passes a sieve made by holes with 50 mm diameter. At the exit char is cooled down using water. Biochar contains approximately 60% of the input power. The produced pyrolysis gas pass though the biomass and reach the top of the reactor and then enter a combustion chamber.

12.1.5. Pyrolysis Plant at Pyreg

The plant is fed with sewage sludge. The pyrolysis reactor is heated by exhaust gases obtained from the combustion of pyrolysis gas. The reactor can be fed with about 1000 tons of dry mass per year [8]. The mass flow rate of biochar out of the plant is constant and the process is continuous.

Carbonization efficiency is up to 60%. The energy efficiency of the entire process is comprised between 90% and 95%. The temperature in the reactor is between (400 to 850) °C depending on the fuel moisture. The pyrolysis gas is combusted in a FLOX-burner, which has high efficiency and high combustion temperature (about 1250 °C). The burner is designed to have low NO_x emissions.

12.1.6. Thermo-Catalytic Pyrolysis

The thermo-catalytic reforming (TCR®) reactor is an electrically heated auger type reactor developed and built by Fraunhofer UMSICHT, Sulzbach Rosenberg, Germany. The TCR®-2 reactor setup consists of a hopper (1) connected to an electrically heated horizontal auger reactor (2) which is followed by a vertical reforming unit (3). Then follows a shell and tube type heat exchanger (4) which

is used to condense vapors coming from the reforming unit. An external chilling unit (5) maintains the temperature of the condenser at −5 °C. The condensation unit (4) is followed by a gravity settler (6) which collects the liquid products coming from the vapors (7). Provisions have been made to collect condensed liquid products from the vapors condensation unit and separation unit via a common condensate collection system (7). Then follows an ice cooled second heat exchanger (8) and a gas cleaning unit (9) for further purification of incondensable gases. After condensation the gas is filtered with: activated carbons (10), candle filter (11) and silica wool filter (12). The exit pipe of the reactor is connected to a measuring unit composed by: gas flow meter (13), online gas analyzer (14) and a gas calorimeter (15). The plant is shown in Fig. 12.4.

Fig. 12.4

TCR®-2 Laboratory plant. Reprinted with permission from [9]. Copyright © 2018, Elsevier

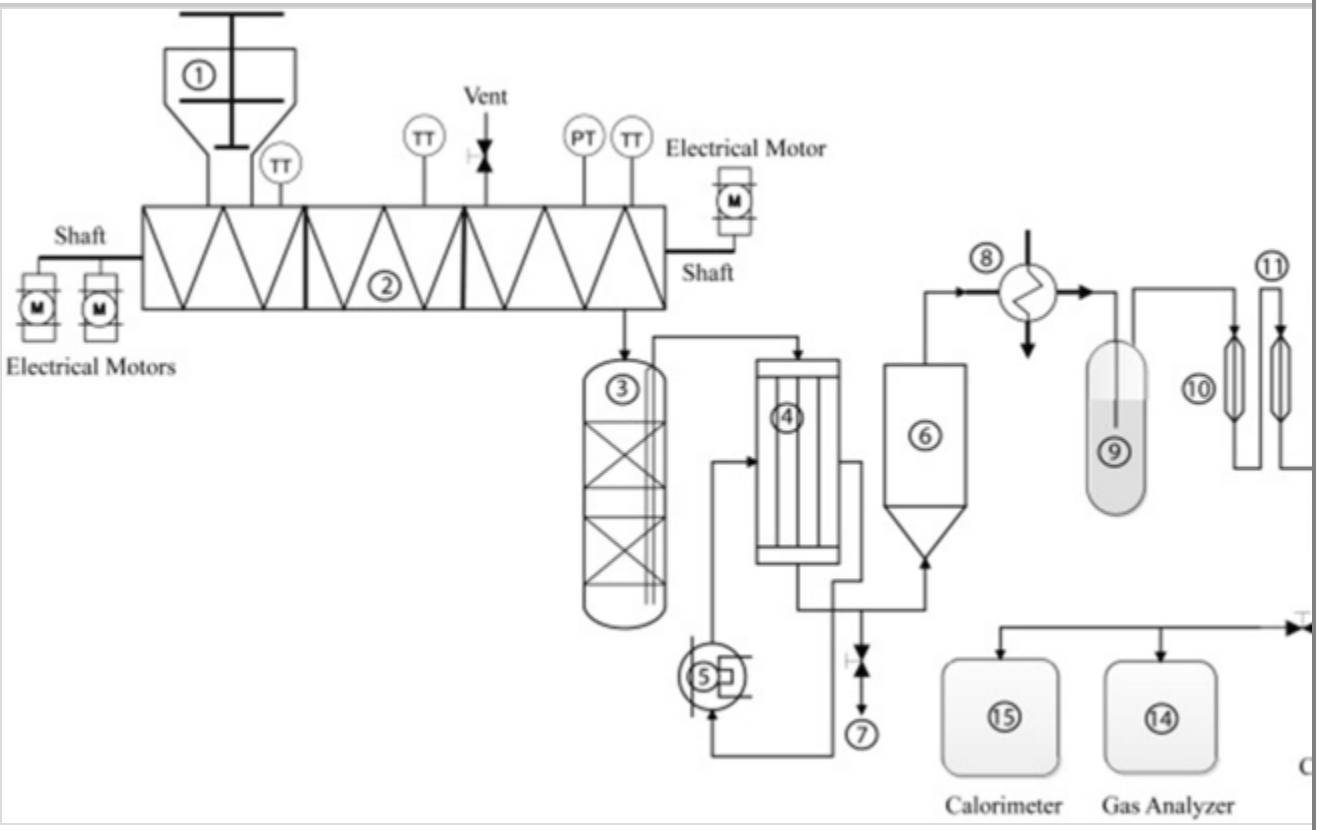

12.1.7. 3R Agrocarbon

The 3R Agrocarbon technology is based on a thermochemical (pyrolysis) process. The main input used is represented by food grade cattle and other types of bone grist. The main output is charcoal to be used as a fertilizer, in that it has a high content of nutrients (P, K, Ca and N). The capacity of the plant is higher than 12,500 t/y. Technology status is very high and can be considered about TRL8/IRL8. In the 3R process the bone grist is heated to as high as 850 °C in the carbonization kiln [10]. Temperature is higher than usual biomass processing temperatures, but it is needed to get high quality products. The main advantage of the technology is represented by feed flexibility. A wide

range of different types of organic material streams can be fed to the reactor which is based on a rotary kiln.

12.1.8. Milena Gasifier

The Milena gasifier design uses the coupling of two reactors: a bubbling fluidised bed (BFB) combustor and a riser reactor. The BFB combustor is used to provide heat externally to the riser reactor where gasification take place. For this reason, the Milena gasifier is an allothermal gasifier [11]. The selection of a riser reactor for the gasification process has a positive effect on cold gas efficiency compared to a BFB, because less dilution gas is introduced into the gasifier. Fluidization gas is required to fluidize the bottom part of the riser, not to create the velocity required for vertical transport of the bed material. The amount of required fluidization gas is mainly influenced by reactor area and this is much smaller for a riser than a BFB reactor. The velocity in the riser required for vertical transport of the bed material originates by the fact that the gas produced during the devolatilization of the biomass adds adds pressure inside the riser and pushes the products of the process out of it.

Compared to other gasifiers, like circulating fluidised bed (CFB) or BFB gasifiers and downdraft gasifiers, Milena gasifier has a higher cold gas efficiency (CGE). Milena CGE in fact is about 80% while the other gasifiers can reach usually 70%. The advantage of the gasifier is that a higher efficiency is achieved at lower temperature and also that the heating value of the producer gas is about (12–15) MJ/Nm^3 (dry gas basis), with a very low content of nitrogen. The syngas is cleaned with the OLGA system.

12.1.9. Güssing Gasifier

The combined heat and power (CHP) plant at Güssing in Austria is a FICFB (Fast Internal Circulating Fluidised Bed) steam gasifier that converts wood chips to a product gas with a heating value of approximately 12 MJ/Nm^3 (dry basis), see Fig. 12.5.

Fig. 12.5

Gasification CHP plant at Güssing. Reprinted with permission from [12]. Copyright © 2013, Elsevier

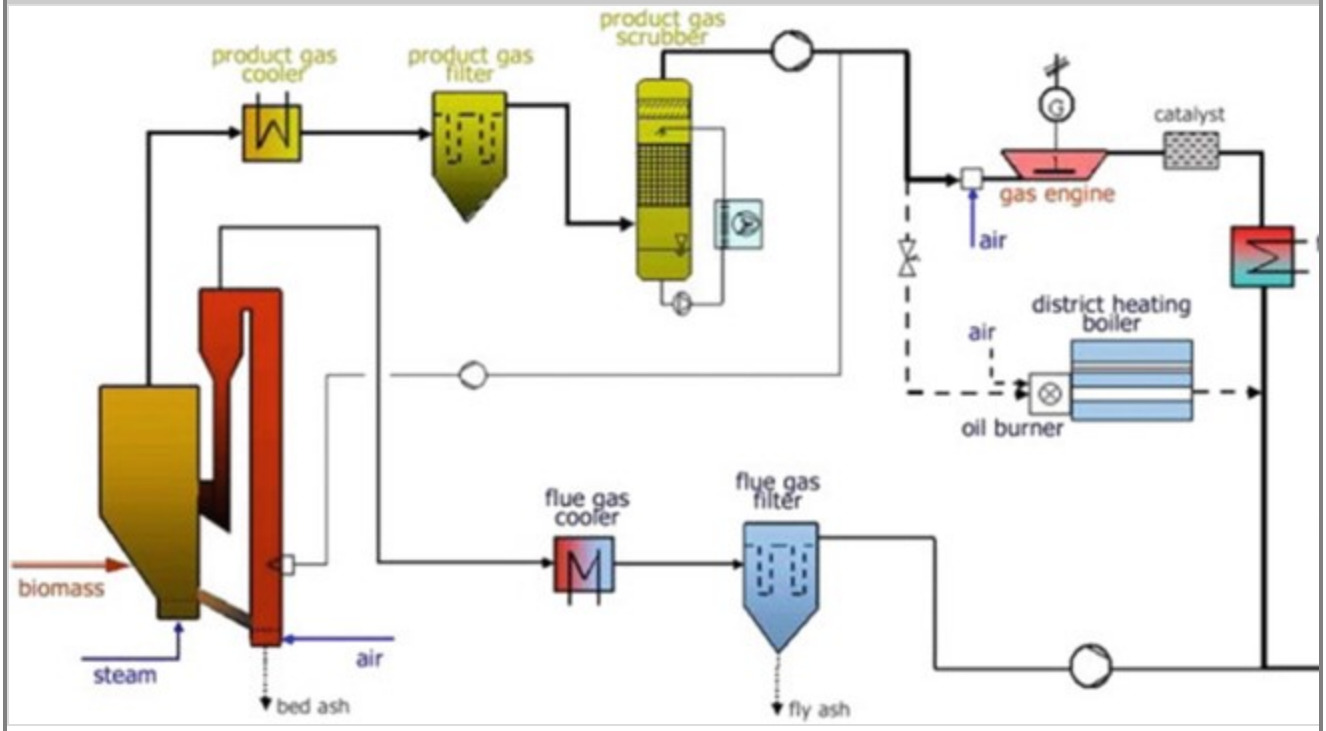

After passing through a cleaning section (two-stage gas cleaning system), the product gas is used as fuel in an internal combustion engine with a generator producing electricity and heat for the grid. If the engine is not in operation, the product gas can be burned in a boiler, producing only heat. The plant is characterized by a thermal input of 8 MW, the electric output is about 2.0 MW, the thermal output is about 4.5 MW and the overall efficiency is about 25%. The FICFB gasifier consists of two zones; a gasification zone and a combustion zone. The combustion zone provides heat through the bed material to the gasification zone. Steam is used as gasification agent; this implies a lower tar content, compared to air-blown gasifiers [13]. Olivine sand is used as bed material. The amount of tar in the raw product gas is about (1500–4500) mg/Nm^3 (dry gas basis). Leaving the gasifier, the product gas is cooled down to a temperature of about (160–180) °C. Then it is passed through a fabric filter, removing particles and part of the tar. After the filter comes a scrubber which uses rapeseed methyl ester (RME) as scrubbing liquid. The spent scrubber liquid is recycled in the gasifier combustion zone. The final tar content of the gas is about (10–40) mg/Nm^3 dry gas. The exhaust gas of the engine is catalytically oxidised to reduce CO emissions. In January 2009, the plant had operated for more than 40,000 h since 2002 [14].

12.1.10. GoBiGas Gasifier

The Gothenburg Biomass Gasification (GoBiGas) plant produces 20.5 MW of bio-methane from an input of 32 MW of wood pellets.

The GoBiGas project currently comprises a 32 MW dual fluidized bed (DFB) gasifier (150 dry tonnes of biomass/day) coupled to a state-of-the-art synthetic natural gas (SNG) synthesis process that produces up to 20 MW of biomethane. The plant has run about 10,000 h [16, 17, 18], see Fig. 12.6 for the process steps.

Fig. 12.6

GoBiGas process steps. Reprinted with permission from [15]. Copyright © 2016, Elsevier

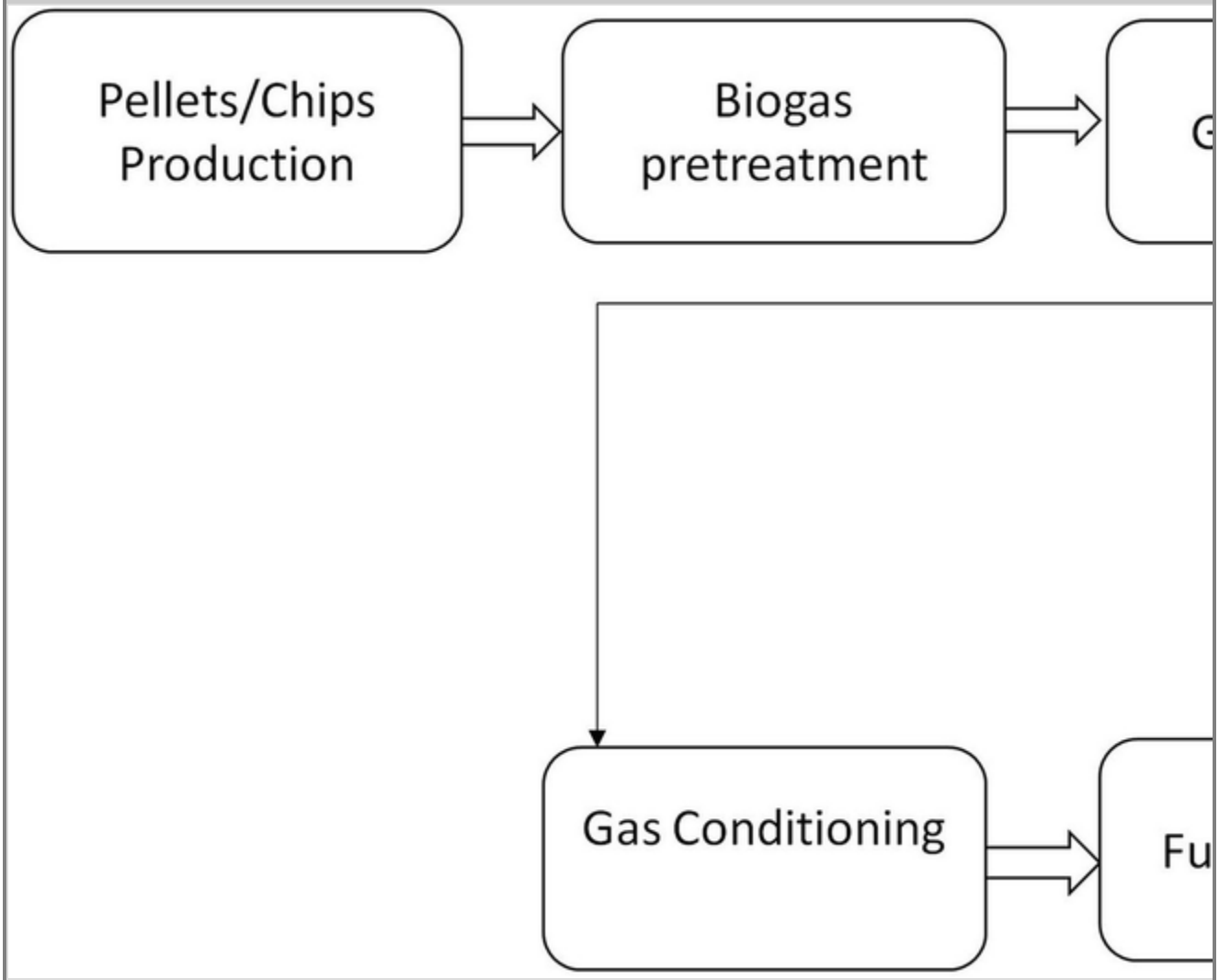

The gasifier in the GoBiGas demonstration plant is one of two, third-generation dual fluidized bed gasifiers which originated from the 8 MW (40 dry tonnes of biomass per day) Güssing CHP plant, which dates back year 2000. This gasifier was followed by the construction of a CHP plant of the same size in Oberwart, Austria [19, 20, 21]. The other third-generation gasifier is a 16 MW (80 dry tonnes of biomass/day) CHP plant in Senden, Germany. A gasification system similar to the one adopted by the GoBiGas is the one developed and built under the TIGAR trademark by IHI Corporation of Yokohama, Japan. This has been later scaled up to a 15 MW (30 dry tonnes of biomass/day) demonstration unit in Kujan, Indonesia and brought into operation in 2015 [22, 23]. In general, the GoBiGas process can be divided into three conversion steps Heat Generation (1); Gasification (2); and Synthesis (3). In addition, there are 2 units for compression (4) and BTX removal (5).

12.2. Production of Pressurized Syngas During Pyrolysis

To produce compressed gas there are two strategies: (i) compression after thermal treatment or (ii) compression during the thermal treatment. Pyrolysis process is influenced by many parameters such as final temperature, heating rate, dimensions of the biomass particles, residence time and pressure. The influence of pressure on pyrolysis product yields and composition has been not fully considered in many studies [24]. In the study of Mahinpey et al. the effect of pressure on the pyrolysis of wheat straw is considered and reported [25]. Experiments have shown that reactor pressure can influence significantly both yields and quality of the obtained pyrolysis products. However, the work of [25] considered a narrow range of pyrolysis pressures, that is, (0.689–2.758) bar. Mahinpey et al. inferred that 1.379 bar is a favorable pressure for the pyrolysis process of wheat straw in a tubular reactor from the point of view of products yield.

Other researchers [26] have worked with an entrained flow reactor fed with pulverized wheat straw and working at pressures of (10 and 20) bar and temperatures of (700–1000) °C. Results have shown that the product yields in this case are not greatly influenced by the operating pressure.

Whitty et al. focused their study on the effect of pyrolysis pressure on char [27] and noted that with an increase in pressure, the particle size of the char obtained from kraft liquors decreased. These results are not confirmed by Mahinpey et al. [25], who used wheat straw as a feedstock.

While the studies on the influence of pressure on biomass pyrolysis products are few, more studies are available on coal pressurized pyrolysis. Roberts et al. [28] found that:

1. yields of coal pyrolysis products (liquid and gaseous) decreased with an increase in pressure, even though the rate of increase was not easy to predict;

2. large differences were found in the morphologies of the chars produced at different pressures;

3. char porosities were greatly influenced by pressure inside the reactor along with char morphologies [29]. Ù

The results obtained for coal cannot be easily translated to biomass, because the bonds between carbon atoms in coal and in biomass substrates are very different. The major components of biomass are cellulose and hemicelluloses and lignin. While cellulose and hemicellulose are characterized by glycosidic linkages between the sugar molecules, lignin is characterized by ether linkages between the aromatic components and between the aromatic functionalities and the phenylpropane components. The energy needed to break these bonds of (380–420) kJ/mol is lower than that needed to break the polycyclic aromatic hydrocarbon structures which are characteristic of some coals. These bonds in fact require about 1000 kJ/mol of energy to be cleaved [30]. These large differences in bond energies that are encountered in the pyrolysis of biomass, compared with that of coal can be studied by analysing the char, its morphology and active sites. In this way also the effect of pressure can be better understood [31]. In the work of Cetin et al. [31] pressurized pyrolysis tests were used with a wire mesh reactor working at high heating rates (500 °C/s), which can reach an internal pressure of about 100 bar.

A typical way to study char morphology is with scanning electron microscopy (SEM) in which porosity and charcoal structure can be analyzed instead recurring to Brunauer-Emmett-Teller (BET) analysis.

Many works in the literature have reported that pressure has an important effect on the composition of pyrolysis products; while it has a negligible effect on their yields which is especially valid for slow pyrolysis. Pressure is an important effect on the porosity of charcoal. In fact, with an increase in pressure, volatiles escape from the pores slower and so tend to remain trapped inside the pores, clogging them and reducing porosity which is a phenomenon that can be detected using NMR spectroscopy and indicates that chars formed at high pressures have an aromatic structure that tend to fuse and collapse in presence of high pressure. Chars formed under high pressure conditions have usually higher carbon content. Figure 12.7a, b show SEM images of samples of char produced from Radiata pine pyrolysis at different pressures [31]. Char samples reported in Fig. 12.7 have been produced using a wire mesh reactor operating under a nitrogen atmosphere. As shown in Fig. 12.7a, char particles have been generated at pressures of (5, 10, 20) bar. It can be seen by comparing Fig. 12.7a-c that generally the cross section image of charcoal obtained at high pressure is characterized by particles that have larger cavities and thinner cell walls, compared with chars that have been generated at low or atmospheric pressure. If pressure is applied, bigger particles are obtained, which are characterized by a perforated surface structure. So with an increase in temperature, the porosity of charcoal collapses leaving space to large voids inside the particles and making cell walls thinner. This means that microporosity is reduced while macroporosity increases with an increase in pressure.

Fig. 12.7

SEM analysis of sawdust pine chars produced under pressure (**a**) 5 bar, (**b**) 10 bar, (**c**) 20 bar. Reprinted with permission from [31]. Copyright © 2005, Elsevier

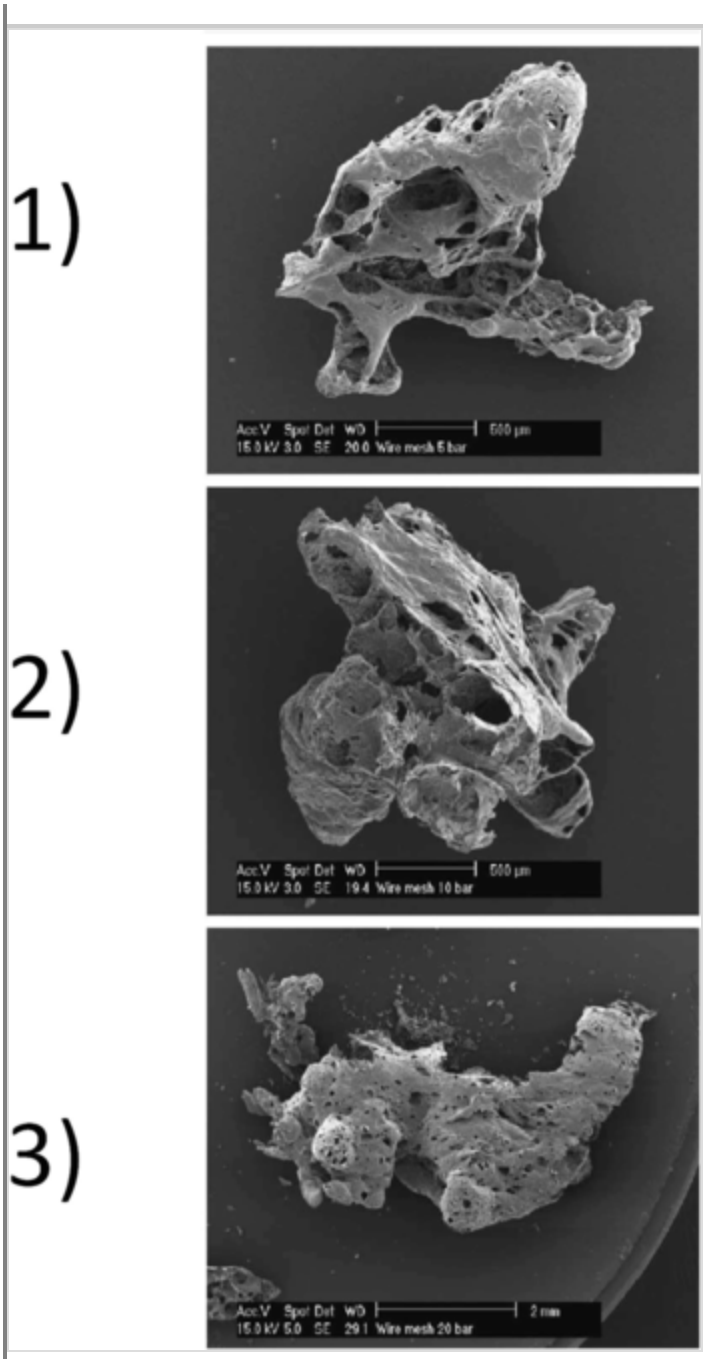

Similar results to those shown in Fig. 12.23 have been obtained with eucalyptus wood [31]. These tests have been performed at 20 bar pressure at different heating rates in the same wire mesh reactor. It has been noted that when high heating rates are used the char particle melts down and loses completely its structure. If the focus is on pyrolysis gas composition, Porada [32] show analysis of the kinetics of gaseous products evolved during coal pressurized pyrolysis, namely, methane, ethane, ethene, propane, propene and hydrogen at (0.1, 2.5, 5.0, 10) MPa. The experiments were performed by heating a 1 g sample of coal with particle size comprised between (0.8 and 1) mm. The heating process was performed in a quartz tube reactor in argon atmosphere, starting to ambient temperature and reaching up to 1200 K at a heating rate of 3 K/min using electric heaters. Pyrolysis gases were cooled down to enable tar and water to condense. The noncondensable gases at the exit of the

condenser were analyzed with the use of gas chromatography: an HP 5890-A type gas chromatograph (GC) equipped with FID for analysis of C_1–C_3 hydrocarbons and another GC equipped with TCD and is used to measure H_2, CO and CO_2. Analysis of the pyrolysis gases have shown that an increase in pyrolysis pressure gives an increase in methane yield and a reduction of hydrogen yield where the C_2 and C_3–hydrocarbons are given by single reactions. With an increase in pyrolysis pressure, an important decrease in the yield of CO and CO_2 occurs.
AQ3

12.3. Syngas Compression

12.3.1. Compressors Classification and Selection

As reported by Blackmer [33] for compressor selection, compression ratio is a key parameter as defined by:

$$R = P_d / P_s \tag{12.1}$$

where P_s represents the absolute suction pressure and P_d represents the absolute discharge pressure. Usually the identification of the compression ratio is the first step in compressor selection, which involves globally the following steps:

1. Calculation of compression ratio;
2. Selection of a single-stage or a two-stage compressor;
3. Calculation of discharge temperature;
4. Determination of volumetric efficiency;
5. Determination of required piston displacement;
6. Selection of compressor model;
7. Determinaton the minimum rpm required of selected compressor;
8. Selection of actual rpm;
9. Calculation of actual piston displacement;
10. Calculation of power required;
11. Selection of appropriate options.

Details on how to address each step are proposed in ref. [33]. Another important aspect to take into account in compressor selection is the type of compressor fulfills better the process requirements. Generally the goal of a compressor is to increase the static or inlet pressure of the gas and deliver it at the specified discharge pressure and flow rate. This can be done by different types of compressors. The two basic categories of compressors are: dynamic (centrifugal and axial) and positive

displacement (reciprocating and rotary types). Table 12.2 shows a summary of typical operating characteristics of compressors. Dynamic compressors are based on the principle that they provide velocity to a gas which passes through impellers or blades. The gas then exits the blades and enters into a stationary volume were its velocity is transformed into pressure. In centrifugal compressors the acceleration of the gas is obtained through the action of one or more rotating impellers, while in axial compressors we find both rotating and stationary. The shaft rotates a drum inside a casing, which is stationary. Between the drum and the casing rows of airfoils are placed, which are either connected to the drum or the casing.

Table 12.2

Typical operating conditions of compressors [34]

Type	Inlet capacity (m^3/h)	Maximum discharge pressure (bar)	Adiabatic efficiency (%)	Operating speed (rpm)	Maximum power (MW)	Application
Dynamic compressors						
Centrifugal	170-850,000	690	70-87	1800 – 50,000	38	Process gas & air
Integrally geared centrifugal compressors	500 – 500,000	350	80	7000 – 50,000	60	Process gas & air
Axial	50,000 – 850,000	17	87-90 +	1500 – 10,000	75	Mainly air
Positive displacement compressors						
Reciprocating (piston)	20 – 34,000	4150	80-90	200 - 900	15	Air & process gas
Diaphragm	0 - 250	1400	60 - 70	300 - 500	1.5	Corrosive & hazardous process gas
Rotary screw (wet)	100 – 12,000	24	65-70	1500 – 3600	1.5	Air, refrigeration & process gas
Rotary screw (dry)	200 – 100,000	1 - 50	55 - 70	1000 – 20,000	6	Air & dirty process gas
Rotary lobe	25 – 50,000	0-3 – 1.7	55 - 65	300 – 4000	0.4	Pneumatic conveying, process gas & vacuum
Sliding vane	15 – 5000	10	40 – 70	400 – 1800	0.35	Vacuum service & corrosive process gas

Type	Inlet capacity (m^3/h)	Maximum discharge pressure (bar)	Adiabatic efficiency (%)	Operating speed (rpm)	Maximum power (MW)	Application
Liquid ring	10 – 17,000	5.5 – 10.5	25 - 50	200 – 3600	0.3	Vacuum service & corrosive process gas

In positive displacement compressors the compressing action is due to a mechanical part which reduces the volume of a chamber. As shown in Table 12.2, an important parameter of the compressor is the efficiency. Different types of efficiencies can be considered, as explained in the next section.

12.3.2. Compression Efficiency

For a compressor the efficiency can be defined as the ratio of output work (head) to input work (shaft power) of a system [35]. The difference between the two works is due to friction and results in a higher temperature at discharge. Assuming negligible heat transfer, minimal velocity effect and an isentropic process, the work can be calculated as follows:

$$W = c_p \left(T_2 - T_1\right) \tag{12.2}$$

which is derived directly from the general energy equation given by the first law of thermodynamics. In Eq. (12.2), W is the work, c_p is the specific heat of the compressed material and T_1 and T_2 are respectively the inlet and the outlet temperature. So, based on this definition, the isoentropic (or adiabatic) efficiency results from Eq. (12.3).

$$\eta_{\text{ad}} = c_p \left(T_{2\text{ad}} - T_1\right) / c_p \left(T_2 - T_1\right) \tag{12.3}$$

where $T_{2\text{ad}}$ represents the isentropic compression temperature and η_{ad} represents the isentropic efficiency. For an adiabatic process for a gas, the following equation applies:

$$\frac{T_1}{T_2} = \left(\frac{P_1}{P_2}\right)^{(k-1)/k} \tag{12.4}$$

where k is the ratio between specific heats and it is a constant, P_1 is the pressure at the inlet and P_2 is the pressure at the outlet. Through mathematical calculation, the denominator of Eq. (12.3) can be written as:

$$T_2 - T_1 = T_1 \left(\frac{T_2}{T_1} - 1\right) \tag{12.5}$$

Substitution of Eq. (12.4) into (12.5) gives:

12.6

where r_p is the ratio between P_2 and P_1. If Eq. (12.6) is substituted into Eq. (12.3), the equation for isentropic efficiency changes into

$$\eta_{\text{ad}} = \frac{T_1 \left[(P_2/P_1)^{(k-1)/k} - 1 \right]}{T_2 - T_1} \qquad 12.7$$

The adiabatic or isentropic efficiency is useful to determine the power of the compressor and its performance. Nevertheless, the polytropic efficiency gives a more accurate efficiency for the compression of an ideal gas. For real gases instead it has to be considered that *k* is not always constant.

Once compression efficiency has been calculated, overall efficiency has to be taken into account [36], defined as the ratio between the adiabatic power (W_{ad}) to the shaft power (W_{sh}), Eq. (12.8):

$$\eta_{\text{overall,ad}} = \frac{\dot{W}_{\text{ad}}}{\dot{W}_{\text{sh}}} \qquad 12.8$$

If a compressor system consists of a compressor, a motor, a controller and other devices, the efficiency of the system has to take into account along with other losses (*e.g.* electrical), that gives:

$$\eta_{\text{sys}} = \eta_{\text{overall,ad}} \bullet \eta_{\text{motor}} \bullet \eta_{\text{controller}} \bullet \eta_{\text{auxiliary}} + \dots . \qquad 12.9$$

12.3.3. Syngas Compression in IGCC Plants

Gaseous fuels derived from thermochemical treatment of biomass, coal and waste are commonly called “syngas”, “pyrogas” or “producer gas”. Usually the word “syngas” is used when the gas final use is the synthesys of useful final products that can be a biochemical or a fuel. Syngas is usually composed of the following gaseous compounds: H_2, CO, CO_2, CH_4, N_2, and O_2 (which is not present in the case of pyrolysis), C_xH_y, traces of tar and water. This gas has, in many cases, a low calorific value and can be burnt in turbines and microturbines. If coal is gasified to produce syngas and then combusted to produce electricity, this results in a more clean process that combusting coal directly as a solid fuel. Syngas can be used also as a raw material, to produce hydrogen and methanol. Gasification is the first process encountered in Integrated Gasification Combined Cycle (IGCC) power plants, which can emit lower quantities of SO_x, NO_x, particulate matter and heavy metals, and have high electrical efficiency [36].

Although IGCC plants have many advantages, they are hampered by economic barriers and technical barriers because it is difficult to operate these plants under fast changing loads. A possible solution to this problem is represented by the compression of the produced syngas and its storage. This technology can grant more flexibility to the plant and widen its field of operation. [37]. If the syngas can be successfully stored, this can help to use it in the power plant only during peak-load demand

and so having higher prices per unit of electricity produced from the distribution system operator [38]. So syngas compression can permit operation of a plant when the price of electricity is more convenient and this increases the IGCC plant profitability (see Fig. 12.8). The compression process is simple but at the same time needs large volumes for storage if the compressing pressure is low, (10–20) bar.

Fig. 12.8

Coal gasification plant with syngas storage. Reprinted with permission from [38]. Copyright © 2012, Elsevier

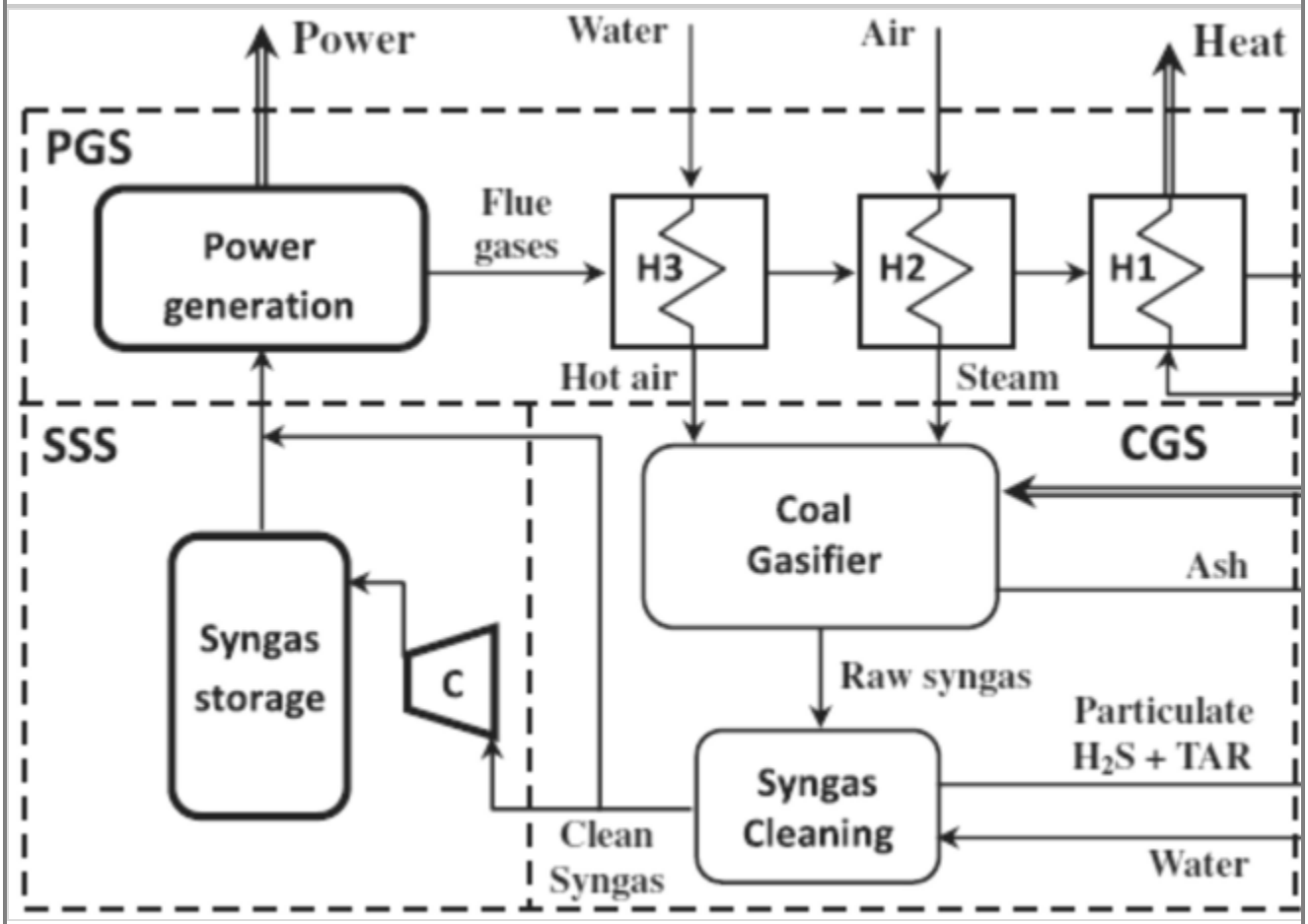

Both volumetric and centrifugal compressors can be used for syngas compression. Volumetric compressors can be used with different ranges of mass flow and different compression ratios. Centrifugal compressors can be operated with higher efficiencies [39]. The two parameters to be considered when designing a syngas storage facility are: power demand and syngas storage capacity. These are directly influenced by the peak energy demand and the conversion efficiency of the IGCC plant [40]. An optimum volume has to be found, given that with the decrease of the storage volume the energy consumption for compression increases (Fig. 12.9).

Fig. 12.9

Energy consumption for syngas compression in function of pressure ratio and isentropic efficiency. System efficiency (η_{SYS}) takes into account the mechanical and electrical energy losses and is assumed to be 95% Reprinted with permission from [38]. Copyright © 2012, Elsevier

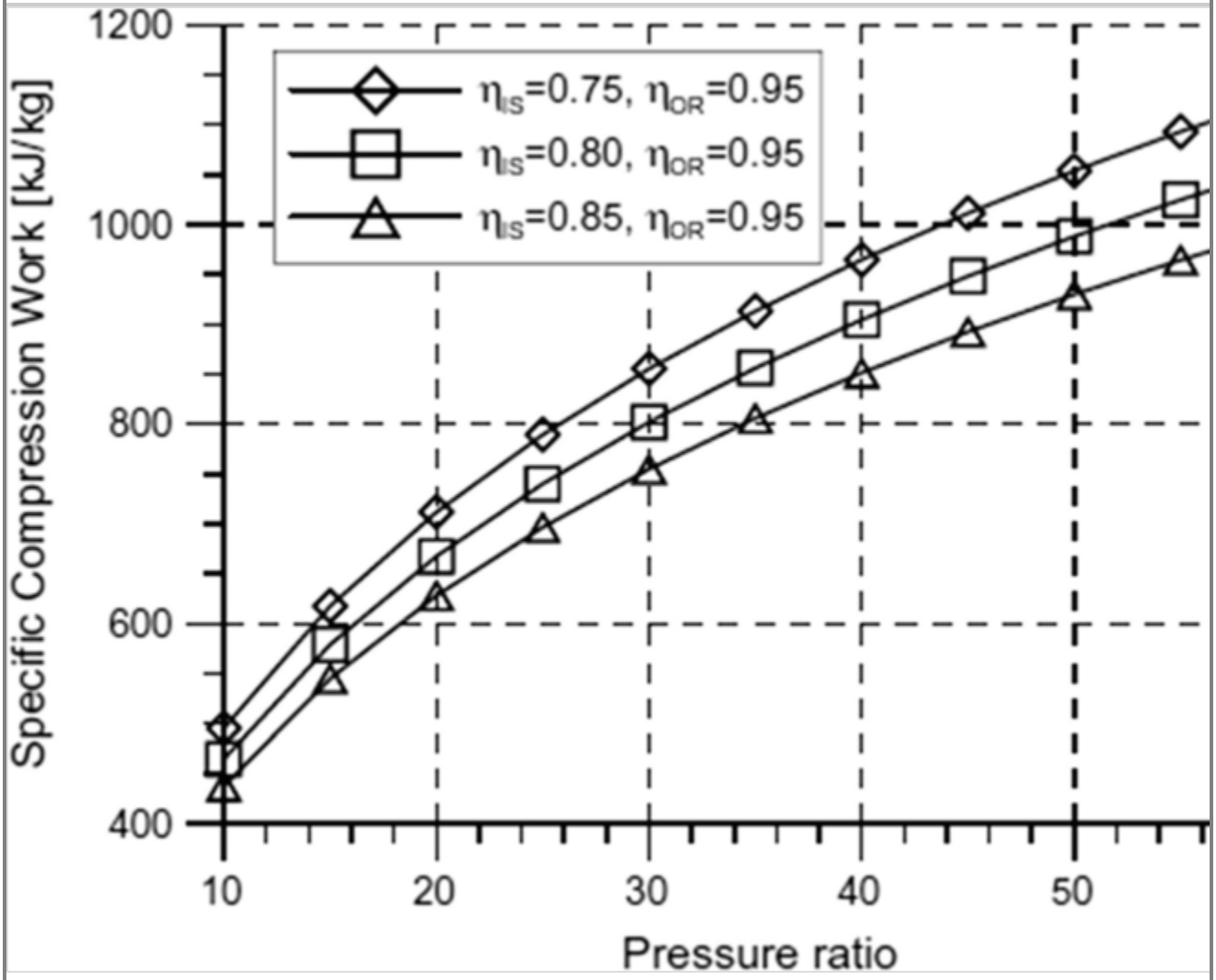

Once the syngas has been produced and stored, to transform it into energy, it has to be burnt in gas turbines, internal combustion engines, combined cycles that couple a gas turbine with a steam turbine recovering the heat released after the exhaust combustion gases have expanded in the gas turbine and fuel cells. Many researchers have studied the energy and economic performance of the different prime movers (see Cau et al. [38]). In this study, different prime movers (i.e gas turbines and internal combustion engines) are analyzed when integrated into a small and medium size coal gasification power plant, in which a syngas storage section is present. The results of the comparison are shown in Table 12.3. The data shown in the Table 12.3 are the result of plant optimization realized in the software Aspen Plus™. Plant performance and load modulation capacity are linked deeply with two parameters: syngas storage ratio; gasifier capacity ratio. The syngas storage ratio is the ratio between the syngas produced in the gasifier section and the syngas stored in the syngas storage section. The gasifier capacity ratio is defined as the ratio between the coal energy input of the IGCC and the coal

energy input of the base load coal gasification plant. The power ratio defined in Table 12.3 is the ratio between the base load power and the peak load power. The peak load energy ratio is the ratio between peak-load and base-load. The Table 12.3 shows that the IGCC configuration using a GT has significantly lower efficiency. This can be explained with the fact that in off-design conditions the efficiency of the gas turbine decreases in a significant way. At design conditions in fact the turbine has an electrical efficiency of 27.1% and a thermal efficiency of 59%. The thermal efficiency is calculated assuming to cool down the exit gases from the turbine from a temperature of 594 °C to a temperature of 120 °C, but what happens in practice is that the turbine works in design conditions only at peak load. In the off-design conditions the performance of the GT results influenced by the load rate. So what actually happens is that in off-design conditions the performance of the GT decreases significantly on the contrary of the internal combustion engine.

Table 12.3

Main performance of Iintegrated Gasification Combined Cycle power plants with gas turbines (GT) or internal combustion engines (ICE) [38]

	IGCC-GT	**IGCC-ICE**
Power ratio	0.6	0.6
Peak-load energy ratio	0.1333	0.1333
Gasifier capacity ratio	1.241	1.201
Syngas storage ratio	0.065	0.075
Overall efficiency (%)	20.6	32.3
Coal energy input (kW)	10980.0	7028.0
Syngas mass flow rate (kg/s)	1.541	0.986
Stored syngas (t/day)	8.65	6.38
Storage volume (m^3)	466.7	344.0
Compressor power (kW)	81.6	60.1
CGS power consumption (kW)	140.1	89.7
PGS power output (kW)	3473.4	3423.0
Base-load power output (kW)	2000.0	2000.0
Peak-load power output (kW)	3333.3	3333.3

The performance of the internal combustion engine is evaluated based on literature data for capacities ranging between (1–5) MWe. The thermal efficiency of the ICE is determined based on heat recovery from exhaust gases, lubricating oil, engine cooling mediums. Generally, the ICE has a higher efficiency at part load compared to the gas turbine.

Once the syngas is compressed it can be used in gas turbines. Here the issue is how to maintain an efficiency comparable to the one which can be eachieved with natural gas, using syngas and without changing turbine materials and design too much. As it is shown in the study of He et al. [41], gas turbines (GT) are designed to be fed with natural gas; if they have to be fed with gases with a lower heating value, the input flow has to be increased, to obtain a Wobbe index which is similar to that of natural gas. The Wobbe index is defined as the ratio between the higher heating value of the gas and the specific gravity. On one hand, if syngas is to be fed to a gas turbine, both the inlet flow and the inlet pressure have to increase; on the other hand, if the pressure ratio is too high, there is the risk of encountering instability at compressor side and too high temperature on the turbine blades.

To respond to the problems caused by the increase of the syngas mass flow other measures can be adopted, such as: air bleed and fuel dilution [42, 43]. Air bleed is compressed air extracted from the compressor, before it arrives in the combustion chamber. Usually bleed air can be used to cool down the gas turbine blades, and to move pneumatic actuators, for example. In this study [42] it is assumed that air bleed is used in an air separation unit (ASU), the nitrogen obtaine from the ASU is fed to the combustion chamber to dilute the fuel. An example of plant layout, where the bleed air is fed to an ASU (which is also fed with the air supplied by the auxiliary air compressor) is shown in Fig. 12.10. The performance of the considered plant can be evaluated based on two fundamental parameters: air bleed ratio and integration degree.

$$\text{Air bleed ratio} = \text{Air to ASU from GT}/\text{Air at GT inlet} \tag{12.10}$$

$$\text{Integration degree} = \text{Air to ASU from GT} / \text{Total air to ASU} \tag{12.11}$$

Fig. 12.10

Gas turbine with air cooling arrangement. Reprinted with permission from [41]. Copyright © 2012, Elsevier

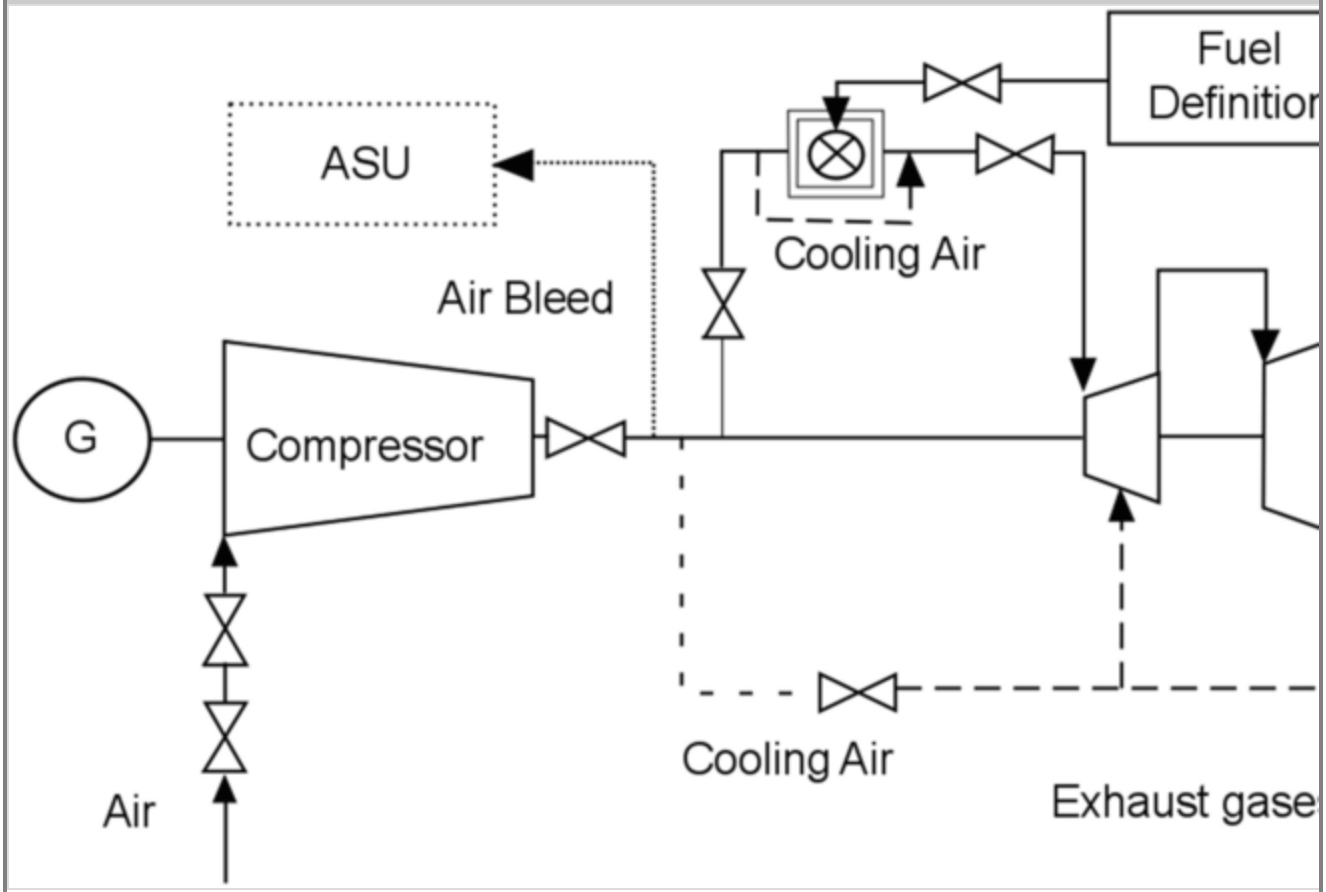

Both air bleed and integration decrease the quantity of exhaust gases flowing through the turbine expander, therefore they reduce the adaptations required in case of an important increase in the volumetric flow through the expander. Many papers have shown that for IGCC plants the recommended integration ratio ranges between (25–30) %, which provides the best balance between the maximum plant electricity production and the efficiency and it does not compromise the reliability and availability of the plant [44, 45]. Generally speaking, in a conventional IGCC plant, the amount of air required at the ASU is about (20–25)% of the air that flows into the GT. The air required by the ASU is directly determined by the oxygen flow required by the gasification reactor. So, an integration degree of (25–30)% determines an air bleed ratio of about (5–7)%.

The injecting of compressed nitrogen coming from the ASU into the fuel gas before combustion is considered a fuel dilution technique; which has numerous advantages, among them the reduction of NO_x emissions and the increase in power production [46].

A possible layout of a gas turbine with air bleed used as a cooling medium is shown in Fig. 12.10. The plant shown in the figure is basically composed by a compressor, a combustion chamber and a turbine expander. The compressor provides two output flows of bleed air which is used as a coolant: one before the turbine inlet and the other behind the first expansion vane. The air entering at the turbine inlet is assumed to do mechanical work, while the air entering after the first vane produces work only in the second rotor [47].

The work of He et al. 2010 [41] calculates the turbine operation window in the case of the plant shown in Fig. 12.10. The window shows the power production from the turbine at different flame temperatures. The change in flame temperature is calculated referring to the operating parameters of the turbine, referring to a E-class GE gas turbine power plant, with the following characteristics: 166.5 MW (power output), 17.6 compressor pressure ratio, 1100 °C turbine inlet temperature, 524 °C turbine exhaust temperature, net efficiency equal to 35.7%.

The operation window of a plant fed with CO-rich syngas, is shown in Fig. 12.11. Figure 12.11a shows the operation window without air bleed and Figure 12.11b shows the operation window with 5% air bleed.

Fig. 12.11

(**a**) Operation window of a diluted CO-rich syngas fired gas turbine without air bleed; (**b**) Operation window of a diluted CO-rich syngas fired gas turbine with 5% air bleed. Reprinted with permission from [41]. Copyright © 2012, Elsevier. Line definitions. (red line): Turbine inlet temperature (TIT); (black line): Blade temperature (Tbl); (pink dashed lines): compressor outlet temperature (TK2) is represented by pink dashed lines; (purple lines): turbine exhaust temperature (TAT)

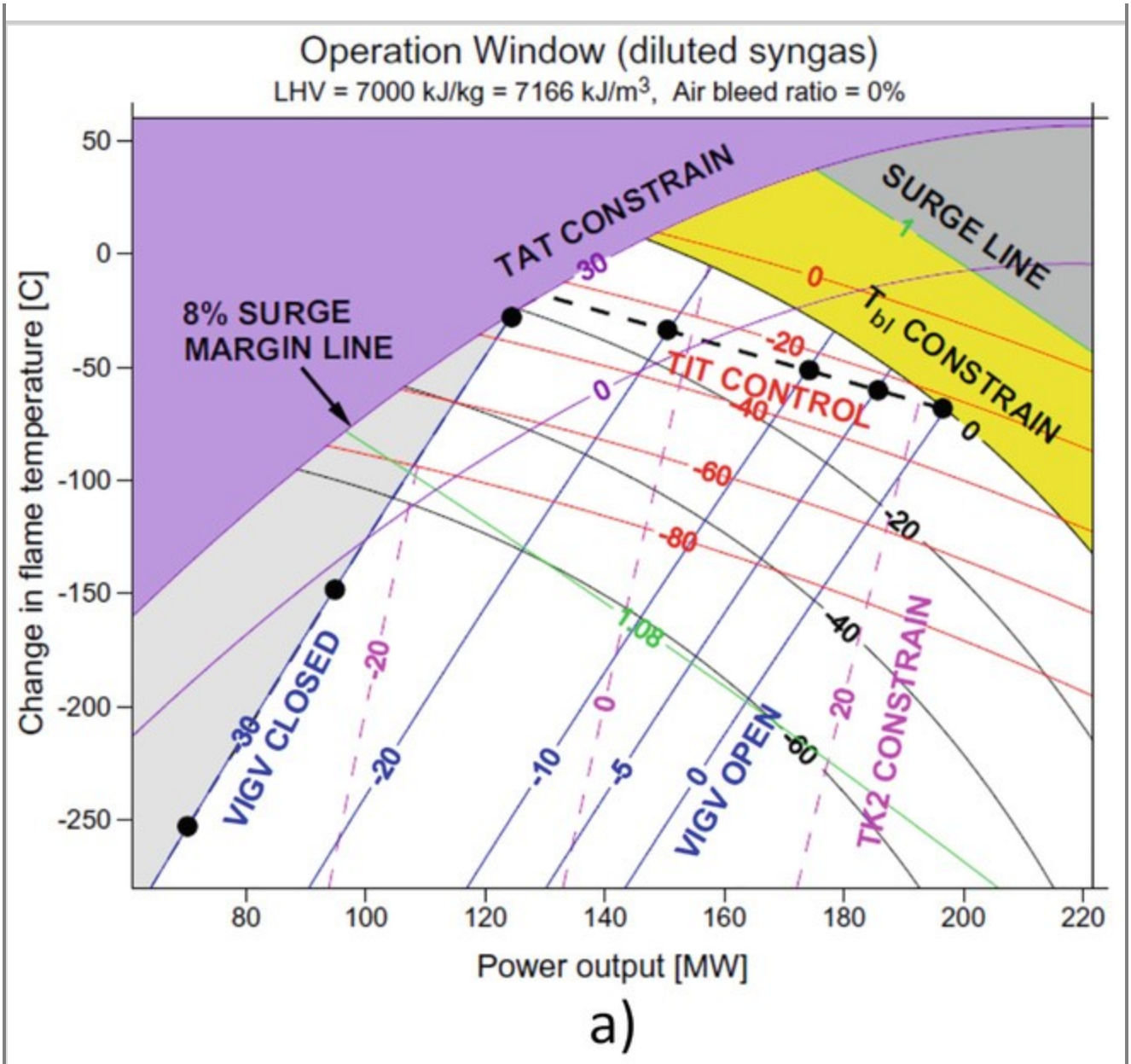

The operational field of the gas turbine at full load is comprised between the 'VIGV = 0' and the "Tbl = 0" contour lines. The Variable Inlet Guide Vane (VIGV), when it is equal to zero it represents the position at the design point, while when it is equal to 30 it refers to a fully closed position where the compressor inlet mass is reduced by 30%.

Compared to the case where the GT is fed with natural gas, given that the syngas has a lower LHV and assuming that the air flow in the compressor is constant, this implies an increase in the fuel mass flow rate to maintain the same flame temperature. Increasing the syngas mass flow rate will cause also the increase of the hot gas mass flow and so the heat output at turbine exit.

Secondly, due to the fact that the volumetric flow of the gas turbine (also known as swallowing capacity) can be changed on a very limited way, the increase in the exhaust gases mass flow can be done only by increasing the compression ratio. If the compression ratio increases then the temperature

of the cooling flow extracted from the compressor also increases. In Fig. 12.11a, it can be seen that if the gas turbine is operated with the design Tbl, the flame temperature will be reduced in an important way. This implies also a reduction of 22 °C of the TIT. It can be seen also that the operating point of the gas turbine approaches the surge line. This is mainly due to the significant increase in the compression ratio. Another important change is that the Turbine Exhaust Temperature (TAT) decreases of about 20 °C, because of the increased turbine expansion ratio. This has as a consequence also an increase in power production of about 16.6%, respect to the design value.

Figure 12.11b shows the results for the scenario using 5% of bleed air extracted from the compressor to produce oxygen in the ASU, this layout is quite common in IGCC plant with partial integration. This new layout is better performing and has many advantages with respect to the previous configuration, among them:

- an increase in the compressor surge margin;
- in this case it is not needed a big reduction of the flame temperature;
- the decrease in the Turbine Inlet Temperature (TIT) is also smaller.

When the gas turbine is operated at full capacity, the power output increases by 8% from design-point value.

If the plant is fed with undiluted CO-rich syngas we will have the operational maps shown in Fig. 12.12a, b. Compared with the case of dilution, non-dilution has a larger operation window. The following positive effects can be noted:

- first of all, turbine blade cooling is remarkably improved;
- the reduction in the TIT, which is necessary to prevent overheat of the turbine blades is less intense. In fact a smaller reduction (about 5 °C) in the TIT is required at full load for a gas turbine with 5% air bleed, compared to the 10 °C which are needed for a gas turbine without air bleed.
- the compressor surge margin is further enlarged. In fact this parameter is about 8% for a gas turbine without air bleed and about 15% for a gas turbine with 5%air bleed.
- the plant can be controlled based on a constant turbine exhaust temperature (TAT) control mode in the load range comprised between 51% and 77% for a gas turbine without air bleed and from 39% to 78% for one with air bleed. This allows to have a relatively higher temperature of the exhaust gases in a wider load range. This can increase the amount of heat which is recovered by the HRSG (heat recovery steam generator).

Fig. 12.12

(**a**) Operation window of an undiluted CO-rich syngas fired gas turbine without air bleed; (**b**) Operation window of an undiluted CO-rich syngas fired gas turbine with 5% air bleed. Reprinted with permission from [41]. Copyright © 2012, Elsevier. Line definitions. (red line): Turbine inlet temperature (TIT); (black line): Blade temperature (Tbl); (pink dashed lines): compressor outlet

temperature (TK2) is represented by pink dashed lines; (purple lines): turbine exhaust temperature (TAT)

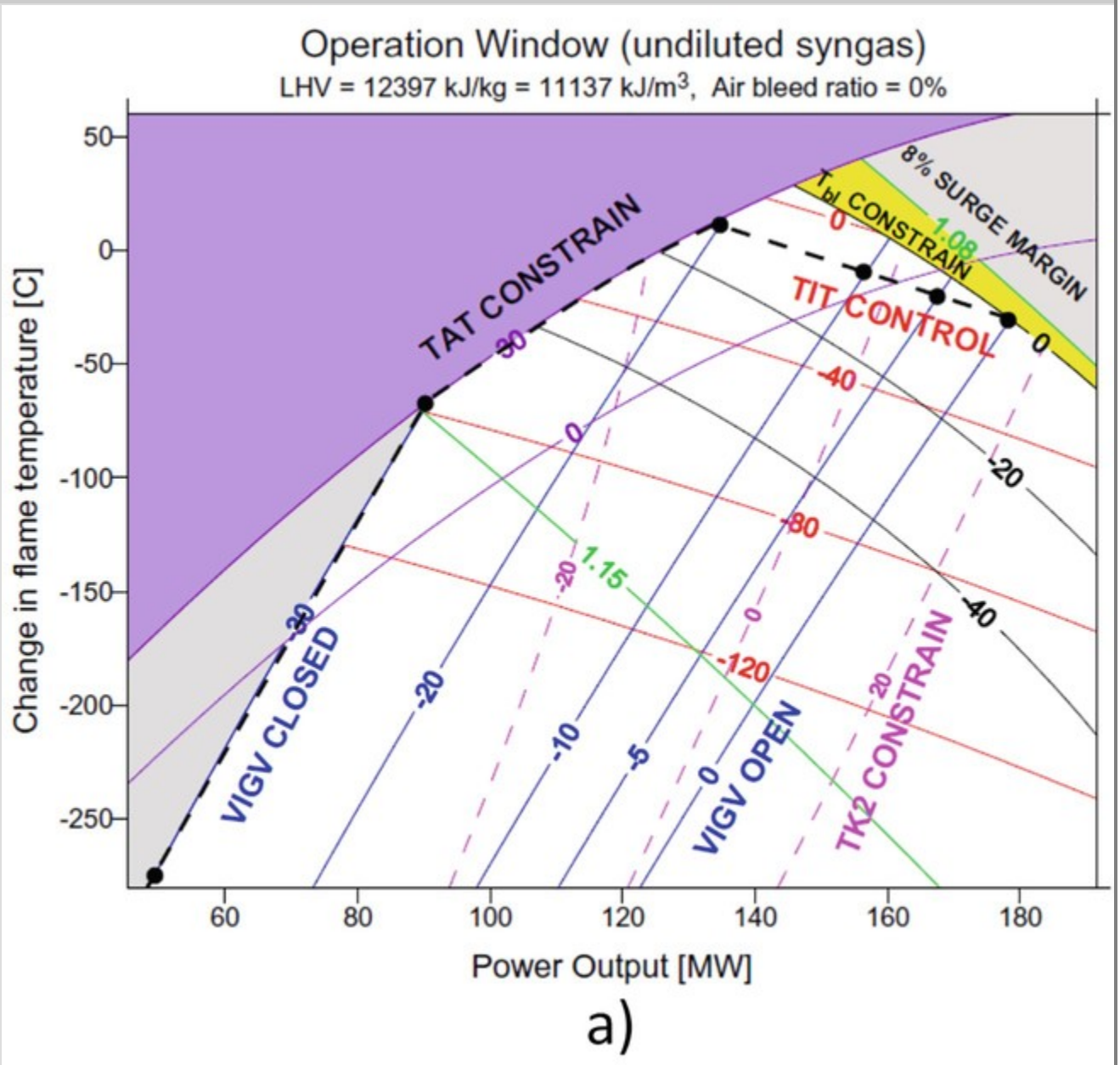

The main disadvantage caused by the operation with undiluted syngas is represented by the fact that the gas turbine has limited possibility to increase the power output given that the undiluted fuel has a smaller mass flow rate compared to the diluted gas.

12.3.4. Syngas Ignition Behavior during Compression

Micro-turbines and gas turbines have been tested using different biofuels in many literature works [48]. Among them: bio-ethanol, bio-methanol, straight vegetable oils, bio-diesel, biogas, hydrogen and pyrolysis oils, syngas, DME.

Despite some difficulties in using syngas in gas turbines (including hydrogen fuel concentrations >90%), many experiments have been performed in various plants all over the world, especially in the United States [49, 50, 51]. Syngas is mainly composed by mixtures containing different concentration of carbon monoxide (CO) and hydrogen (H_2) concentration affect the variation of the syngas mixtures [50]. The variation in syngas composition can complicate the turbine design and operation. Hydrogen can increase the temperature in the combustion chamber, leading to important nitrogen oxide (NOx) emissions. The actual dry low-NOx gas turbine technologies cannot easily support high mass flow rates and fuel concentrations between 15% and 40% [49, 51]. Thus, firing diluted syngas, typically using nitrogen (N_2) or steam in the dilution, can be a good approach [52]. Gas turbines operated in lean premixed combustion conditions can overcome the problem of high emissions and low efficiency. The new concept of syngas turbines is focused on such premixed systems. For premixed operation, there could be concerns over pre-ignition, flashback and safety and performance problems.

Some important publications on the use of H_2 and CO_2 mixtures on GTs are represented by [52, 53, 54, 55]. There are also many studies on developing revised H_2 and CO reaction mechanisms which will be explained on Sect. 12.4.1 [56, 57, 58]. However, lack of data at elevated pressures and temperatures and use of non-dilute fuel/air mixtures make reaction kinetics of syngas blends widely unexplored at conditions relevant to gas turbine applications.

Walton et al. [59] gave an important database of combustion kinetic benchmarks for syngas combustors at typical conditions of temperature and pressure. The study has been done to understand properly the ignition behavior of the simulated syngas mixtures as a function of combustion conditions and syngas composition. To analyze high temperature and high pressure combustion phenomena the use of rapid compression facilities (RCF) can be beneficial. These are test benches which are used also for internal combustion engines, because their piston compresses the test-gas mixture in the chamber, in a similar way to what happens in an internal combustion (IC) engine, leading to a very rapid increase in pressure and temperature. These facility can be used also to analyze the behavior of gas turbines combustion chambers.

Different tests have been realized at the rapid compression facility (RCF) of the Michigan University (see Fig. 12.13) [60].

Fig. 12.13

Depiction of the Michigan University rapid compression facility in operation. Reprinted with permission from [60]. Copyright © 2004, Elsevier

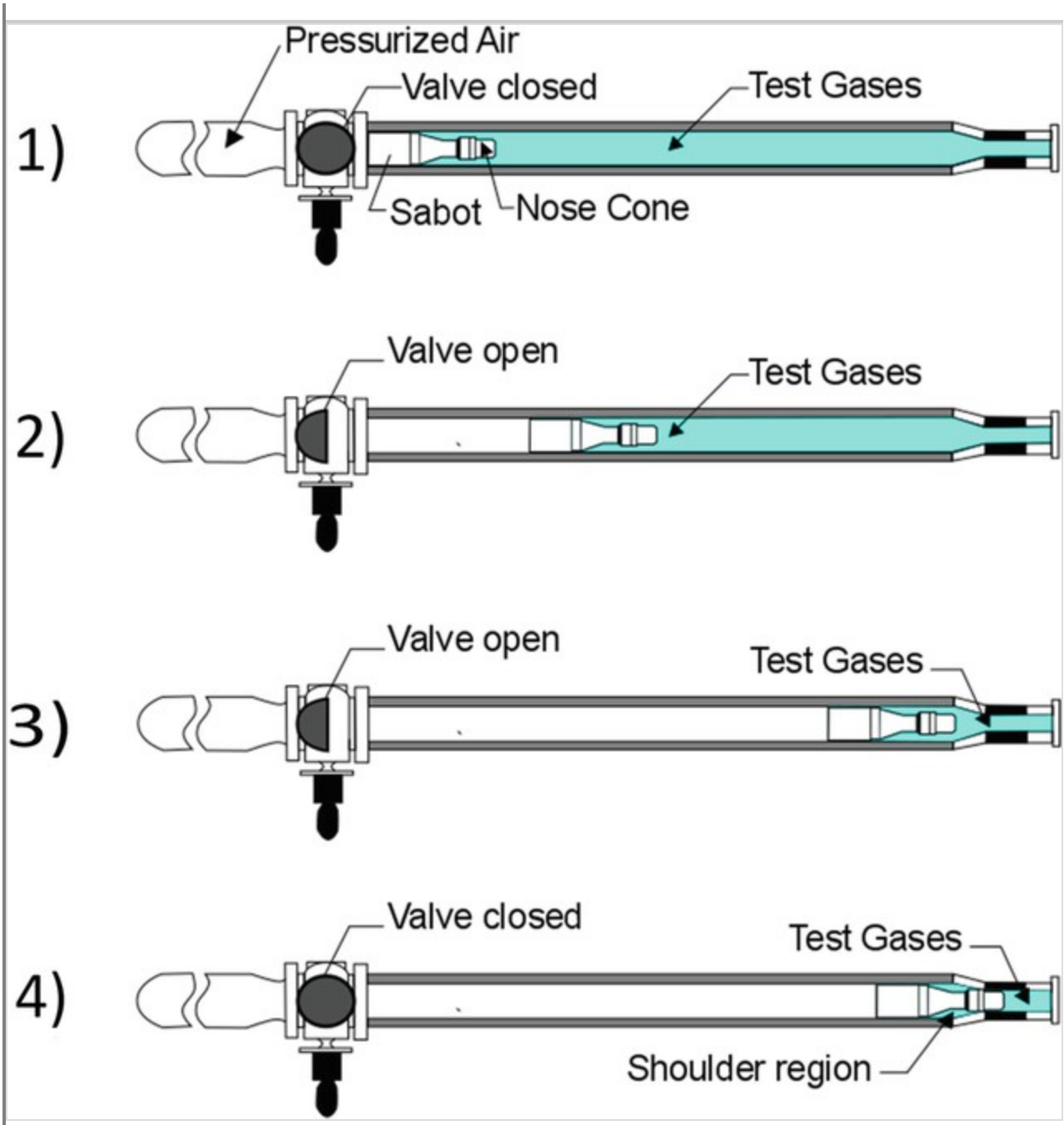

The UM-RCF is mainly composed of the following:

- a driven section, that is where the syngas is contained and compressed;
- the test manifold, where the compressed syngas is stored at uniform high pressure and high temperature conditions;
- the driver section, that is where compressed air is contained and used to drive the sabot;
- the hydraulic control valve assembly; which liberates the compressed air;

– the sabot (free piston), which is driven by compressed air.

Pressurized gas is used by the UM-RCF to move the sabot down the bore of the driven section. The test syngas is loaded in front of the sabot, into the driven section and then it is compressed when the sabot traverses the driven section length.

The phases in which a compression test is divided are:

1. loading of the gas in the driver section. Driver section is loaded with pressurized air.
2. The hydraulic valve is opened to allow compressed air to exit the driver section and to push the sabot along the length of the driven section.
3. the sabot moves through the driven section compressing the syngas ahead of the sabot.
4. the sabot arrives to the end of its movement and traps the syngas in the test manifold.

In detail it can be said that before starting each test a diffusion pump makes the void in the driven section. To begin the experiment the hydraulic control valve and a sheet of polyester film (0.05 mm thick, Mylar®) are used to separate the driver and driven sections. When the driven section is charged with the gas mixture, the hydraulic control valve opens and the high-pressure gas, coming from the driver section, breaks the polyester film, enters the driven section and accelerates the sabot. In the driven section, the test gas mixture compression is done in front of the sabot. When, the sabot nose cone seats by an annular fit situated in the test manifold wall, the compressed test gas is sealed within the test manifold. The compression process can be considered isentropic.

The University of Michigan (UM) used the rapid compression facility (RCF) to perform ignition experiments to analyze the chemical kinetics related to the syngas combustor operation. The UM-RCF is an effective experimental apparatus that can be employed [60] to create constant high-temperature (T = 500–3000 K) and high pressure (P = 0.5–60 atm) conditions. The test facility recreates an environment which is typical of GTs working conditions. The test bench can be used to analyze the ignition delay time (τ_{ign}) of the syngas. This parameter is the most important kinetic characteristic of the combustion process and it is strongly influenced by the syngas chemical composition and also by the temperature and the pressure conditions.

The τ_{ign} value obtained from the experiments is of fundamental importance to indicate the extent of the reaction kinetics and to verify detailed, skeletal and reduced kinetic schemes [56, 58, 61].

With the RCF test bench different kinds of syngas with different H_2:CO ratios (ranging from 0.25 to 4.0) can be tested. Also different syngas dilution rates can be tested by mixing N_2 with syngas; so that the behavior of syngas can be analyzed at high pressures and lean or stoichiometric conditions. These experiments are of paramount importance to design modern gas turbines. In the study of Walton et al. 2007 [59], to simulate the ignition behavior of syngas mixtures consisting of CO and H_2, different parameters have been analyzed, such as: the H_2:CO ratio, the equivalence ratio, the oxygen concentration, the pressure and the temperature. The pressures derivative time-history and the pressure time-history for both pure H_2 and pure CO ignition experiments of the ignition are shown in Fig. 12.14; those data can be compared with the data reported in [62].

Fig. 12.14

Typical experimental results for pressure and pressure derivative time-histories for experimental conditions of T_{eff} = 1004 K, P_{eff} = 11.3 atm, H_2:CO ratio = 0.4, inert:O_2 ratio = 3.76, syngas fuel = 20% H_2, 80% CO. Reprinted with permission from [59]. Copyright © 2007, Elsevier

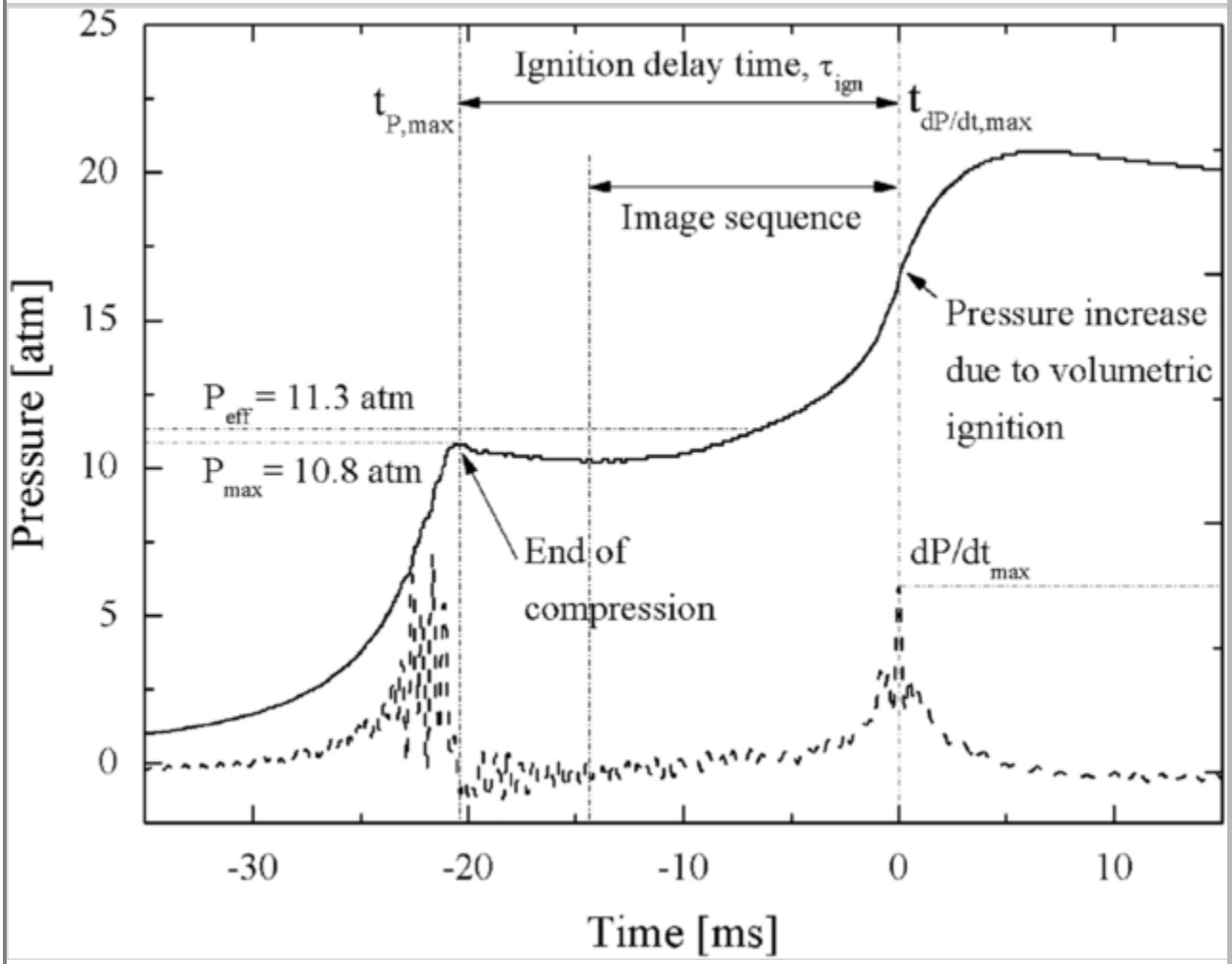

The first peak in the pressure curve shows the end of the compression phase. The pressure remains practically steady for a while, after the gases are sealed in the test section. This stabilization phase is followed by a fast rise in pressure, which coincide with the ignition of the syngas (set as t = 0 s in Fig. 12.14). After the time of ignition the pressure data show an increase in the pressure, which is slow at first and then is followed by a rapid increase. The rapid increase in pressure is due to the presence of reaction fronts before the volumetric ignition. The τ_{ign} is given from every test as the time between Pmax at the end of compression and the maximum value of dP/dt (Fig. 12.14). Repeating the tests in different conditions and with different syngas composition and measuring the ignition delay time for all the cases, a database of ignition times can be produced. Through regression analysis the ignition delay time has been calculated by Walton et al. 2007 [59], as shown in Eq. (12.12).

$$\tau_{\text{ign}} = 3.7 * 10^{-6} P^{-0.5} \phi^{-0.4} \chi_{O_2} * \exp\left(12,500/\overline{R}_{[\text{cal/mol/K}]} T\right) \quad (12.12)$$

where,

- P is the pressure;
- ϕ is the equivalence ratio;
- χ_{O2} is oxygen mole fraction;
- $\overline{R}_{[cal/mol/K]}$ is the universal gas constant.

In the ignition tests previously reported in literature and performed on hydrogen and hydrocarbons, when shock tube and rapid compression facilities have been used, similar phenomena of creation of localized reaction fronts and propagation to the entire combustion chamber have been noticed [63, 64, 65, 66, 67]. This phenomenon is depending on syngas composition. The reaction front propagation is absent in the case of lean mixtures (with fuel mole fractions below a critical limit), above a limit of fuel concentration ignition fast propagation becomes observed (Fig. 12.15).

Fig. 12.15

Comparative of experimentally measured H_2 and CO ignition delay time with model predictions as a function of inverse temperature. The experimental data have been normalized to P = 15 atm, ϕ = 0.4, χ_{O2} = 18% using Eq. (12.12). Reprinted with permission from [59]. Copyright © 2007, Elsevier

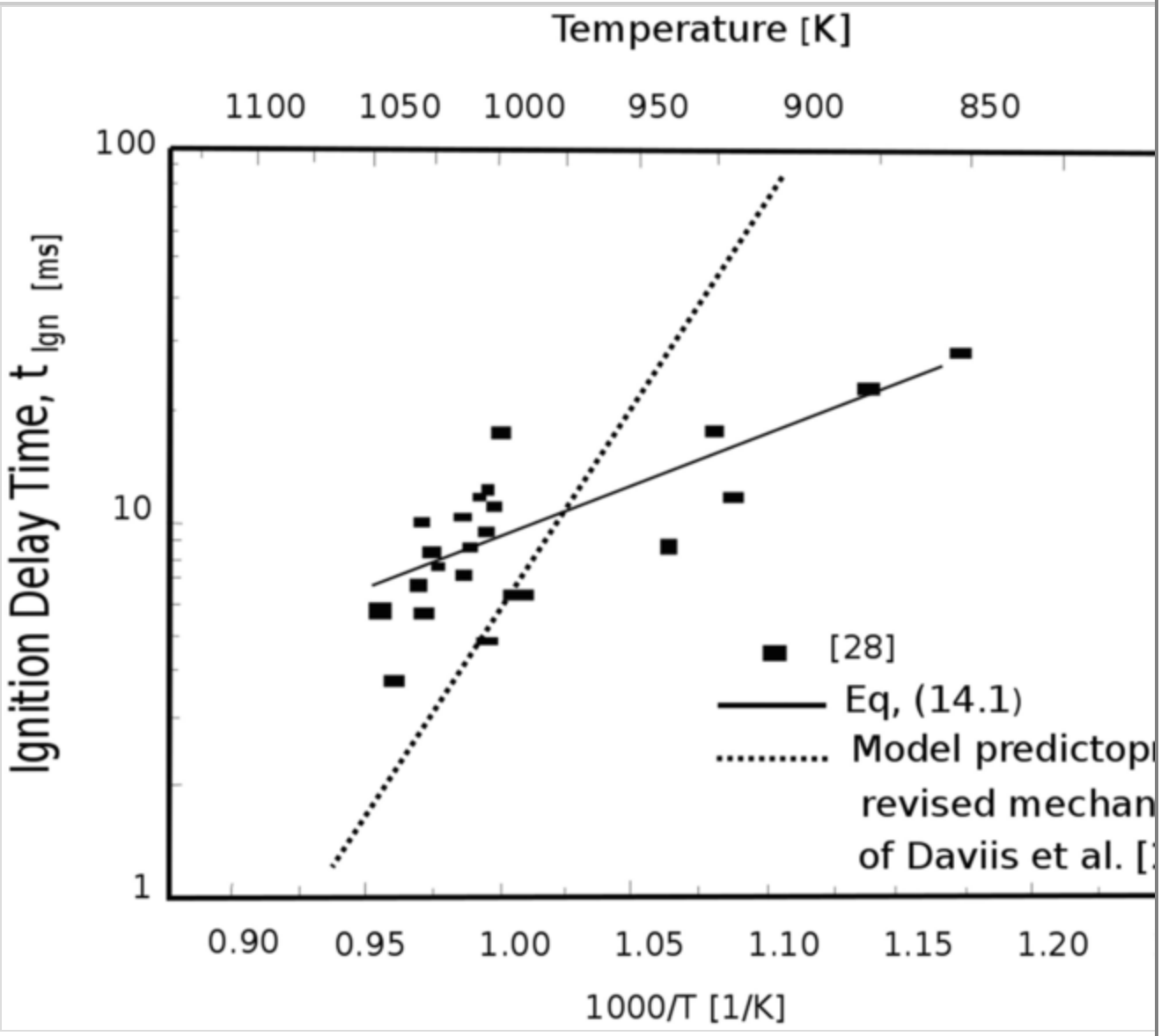

AQ4

Ignition delay time can be also described by the kinetic mechanism developed by Wang and co-workers [57, 68]. This derives from the mechanism previously developed by Davis et al. [57], which is based on the work of Mueller et al. [56].

The scheme of [56] was re-evaluated by Davis et al. [57], updating it with reaction chemistry and thermodynamic data to obtain results which were more correspondent to the experimental conditions.

Figure 12.21 shows the complete dataset of experiments performed by [50]. The results of ignition delay time are plotted against 1000/T. The results are also interpolated with Eq. (12.12). This kind of interpolation is also compared with the model of Davis et al. [57]. It can be seen that the interpolation had a better performance than the model of ref. [59].

12.3.5. Syngas Homogeneous and Heterogeneous Ignition

In combustion processes we can have premixed flames and diffusion flames. Diffusion flames in particular can be classified as homogeneous and heterogeneous. In homogeneous flames the characteristics are determined by the flow of gases and by interdiffusive phenomena; while in heterogeneous flames the characteristics are determined by the exchange of heat and material with the surface of the solid. An important study authored by Chaos and Dryer [69] has evaluated the recent research on chemical kinetics of syngas combustion. The study presents a critical comparison of the differences between kinetic model predictions and experimental measurements in high-pressure ignition tests.

Auto-ignition can be of two types: strong and weak [70]. Weak ignition is defined as non-uniform ignition of the mixture; while strong ignition is defined as a phenomenon which starts with a wave that propagates through all the combustible mixture.

Voevodsky and Soloukhin have been the first to study this phenomenon [71]. They arrived at the conclusion that the weak ignition can be explained with a kinetic phenomenon which is delimited by the second explosion limit. Thereby, the chemical kinetic process in determining the behavior of ignition is essential.

Meyer and Oppenheim [72] linked the weak ignition to the post shock temperature in the shock tube reactor. Assuming stoichiometric H_2/O_2 mixtures, the following equation for the ignition delay time can be inferred:

$$\left.\frac{\partial \tau_{\text{ign}}}{\partial T_5}\right|_{p_5} = -2\,(\mu\text{s/K}) \tag{12.13}$$

where T_5 and p_5 are temperature and pressure in the shock region. The interesting conclusion of Mewer and Oppenheim [72] is that weak ignition is a phenomenon linked with the dynamics of the gases and it is induced by perturbations to the flow-field.

To understand better the results of [71, 72], in Fig. 12.16 are proposed the data of the study of [71, 72] on weak and strong ignition of different syngases (obtained from mixtures of H_2 and CO in different concentrations). From Fig. 12.16 it can be seen that the sensitivity criterion developed by Meyer and Oppenheim (reported in dashed lines) performs better in predicting the weak ignition boundary than the second explosion limit, especially in the low-pressure region.

Fig. 12.16

Weak and strong ignition limits as a function of temperature and pressure for a H_2/O_2 stoichiometric mixture. Reprinted with permission from [70]. Copyright © 2014, Elsevier

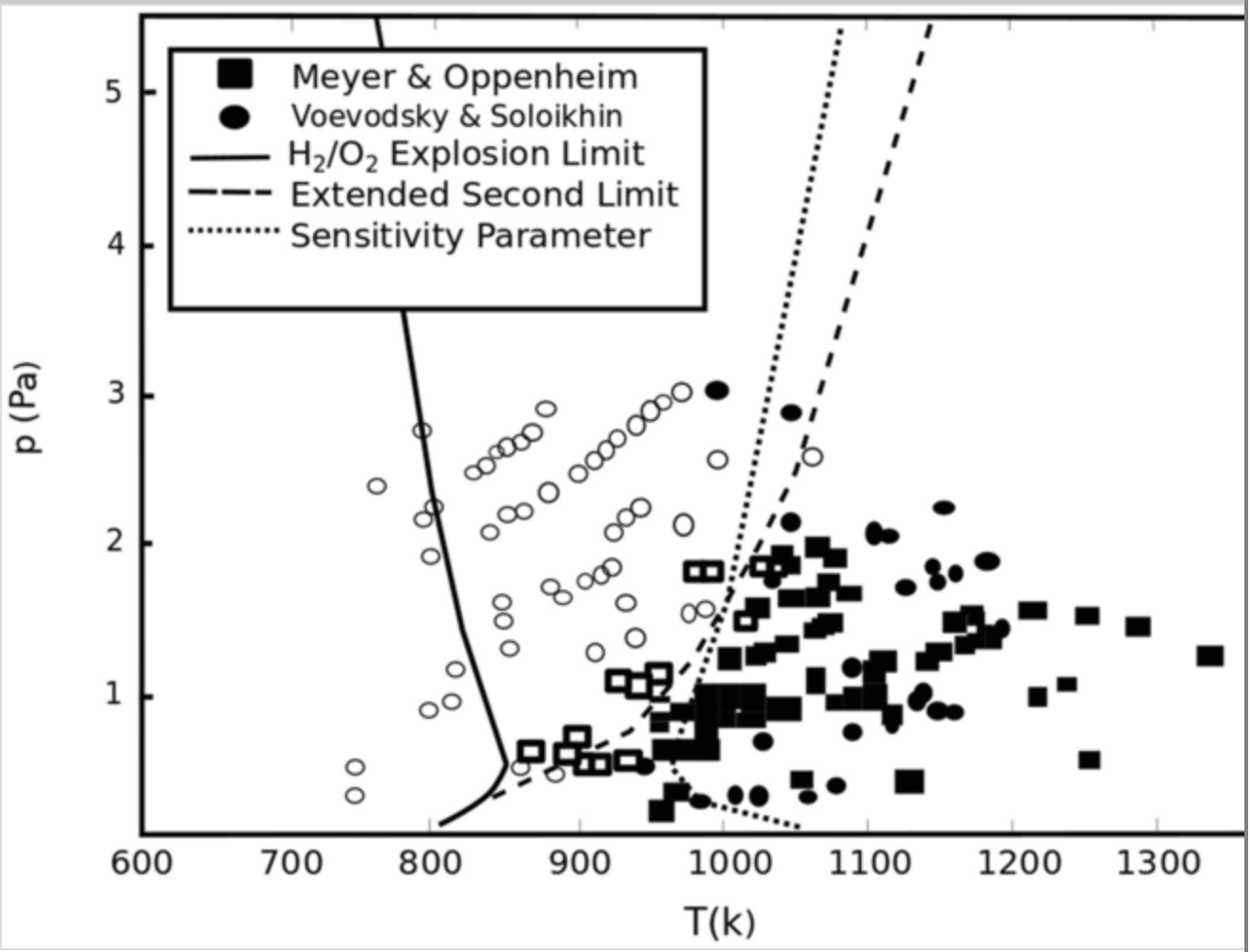

In the work of Mansfield and Wooldridge 2014 [73] an experimental campaign has been conducted to analyze the ignition delay of syngas, differentiating between strong and weak ignition.

From Fig. 12.17 it can be seen that the strong ignition is located usually at temperatures which are higher than 1000 K. The strong ignition limit is not existent anymore at high pressures, where it has been assessed only strong ignition (i.e homogeneous ignition).

Fig. 12.17

Ignition behavior as a function of thermodynamic state for mixtures with equivalence ratio equal to 0.1. The strong ignition limit is shown as a hashed area. H_2/O_2 explosion limits are shown as solid lines with upper and lower bounds shown as dashed lines, representing uncertainty in the rate coefficient of reactions Reprinted with permission from [73]. Copyright © 2014, Elsevier

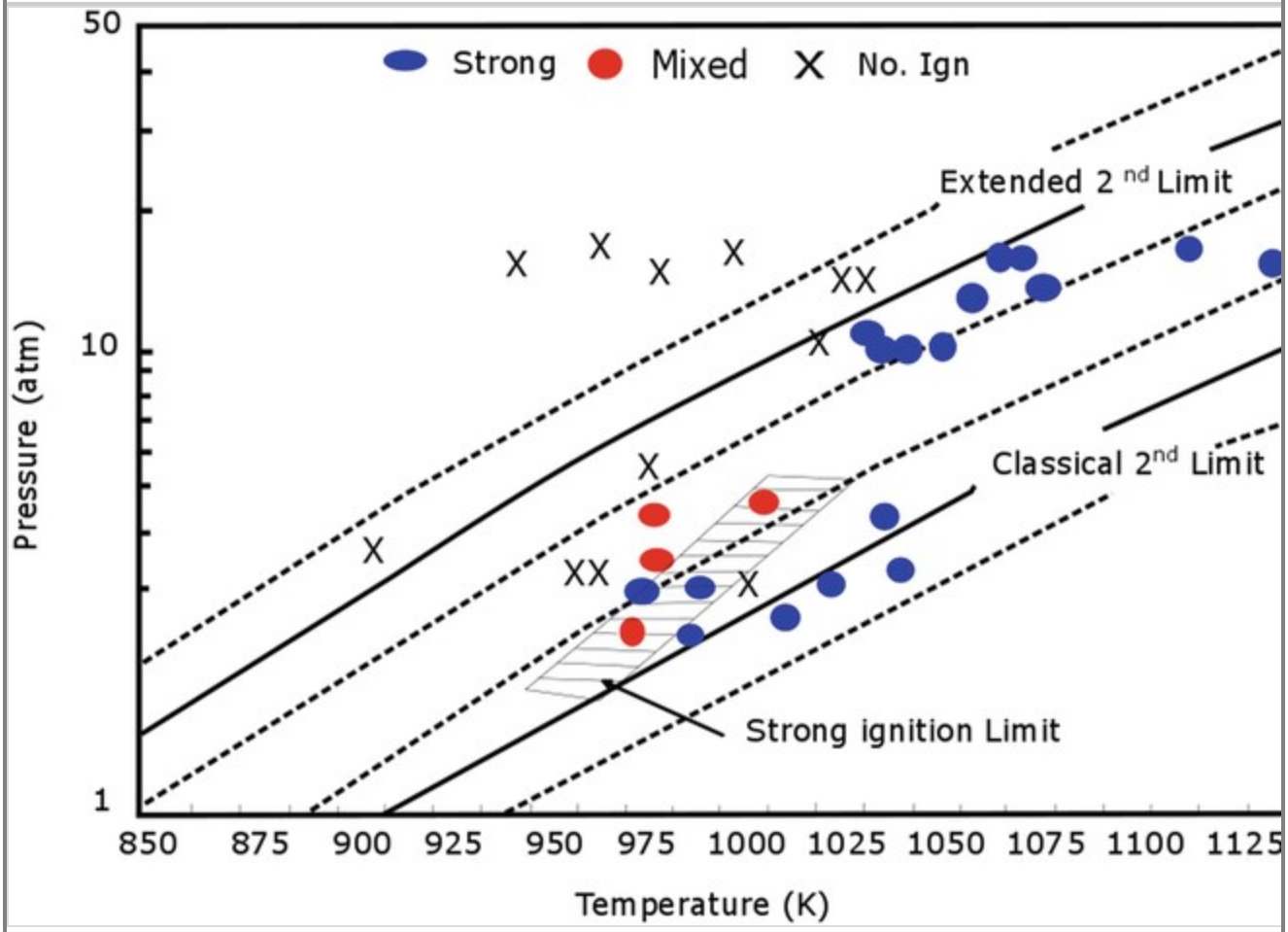

Figure 12.17 shows two explosion limits:

- the second explosion limit and
- the extended explosion limit.

The second explosion limit represents the competition between the dominant chain-branching combustion pathway and the dominant chain-terminating pathway. The extended second explosion limit is defined as the state in which no net radicals (H, O, OH, HO_2) are produced. In this case also HO_2 chemical reactions are included, which are only significant at pressures higher than 1 atmosphere.

12.4. Combustion of Pressurized Syngas in Gas Turbines

12.4.1. Modeling Aspects

Syngas is highly variable in composition. Given that major gaseous components are always the same, i.e. H_2, CO, CO_2, CH_4, N_2 and eventually O_2; the percentage content of those gases can be very different, depending on thermochemical process conditions (final temperature, heating rate) and on

the use of reagents, like steam. The variable composition of syngas influences substantially the combustion behavior both in steady state transient regimens [74].

Generally syngas composition has an important influence on:

- combustion instabilities (different instabilities can happen during combustion, for example: acoustic instabilities, shock instabilities, fluid-dynamic instabilities, chemical-kinetic instabilities, diffusive-thermal instabilities, hydrodynamic instabilities, feed-system interactions, exhaust-system interactions etc.)
- blowoff (flame blowoff can be indicated also as static instability, this happens usually due to a change in the composition of the syngas-oxidizer mixture or in the flow environment of the flame);
- blowout (when excessive flow of oxidizer quenches the flame);
- flashback (upstream propagation of the flame back to the burner);
- pollutant emissions (CO, CxHy, PM, NOx, PAH, etc.);
- flame structure (which can be mainly analyzed based on the shape and on the colors of the flame).

Combustion instability is an important topic for gas turbines, which are usually designed to reach very low emissions levels and so are often operated in conditions which are quite close to the blowout limits. Flashback is also an important instability generated by high flame speed fuels which contain high hydrogen levels.

Given the wide variety of composition of syngas it has to be taken into account that a system designed for a low hydrogen containing syngas cannot be easily adapted to work with a high hydrogen content syngas.

To reduce combustion instabilities much modeling work has been performed, based on kinetic studies. These have been developed to characterize the combustion behavior of H_2/CO mixtures which can be used to model the behavior of syngas [48, 75, 76, 77, 78]. Studies have been performed using both approaches: experimental and modeling. Modeling can also play an important role in emissions reduction. Burning hydrogen rich syngas higher combustion temperatures are obtained and this can cause an increase in NO*x* emissions. For this reason the current approach is to dilute syngas using N_2 or steam [58]. So to reduce emissions a possible solution can be a lean premixed turbine operation, here combustion modeling can be used to check safety issues. For this purpose, very reliable kinetic models are needed. The development of kinetic mechanisms of syngas combustion is a key step toward the optimization of syngas fed gas turbines [75].

Several works are available in the literature on syngas combustion modeling, as presented in Table 12.4.

Table 12.4

$CO/H_2/O_2$ mechanism with rate coefficients in the form $k = A \cdot T^n \cdot \exp(-Ea/RT)$, A units: mol/L/s/K; I units: cal/mol [74]

Number	Mechanism	Species	Reactions
1	NUIG-NGM-2010 [80]	15 species (obtained from an original number of 293)	41 reactions (obtained from an original number of 1593)
2	Kéromnès-2013 [81]	15 species (obtained from an original number of 17)	49 reactions
3	Davis-2005 [48]	14 species	38 reactions
4	Li-2007 [82]	15 species (obtained from an origi nal number of 21)	45 reactions (obtained from an original number of 93)
5	USC-II-2007 [83]	14 species (obtained from an original number of 111)	48 reactions (obtained from an original number of 784)
6	SanDiego-2014 [84]	15 species (obtained from an original number of 50)	37 reactions (obtained from an original number of 244)
7	CRECK-2012 [85]	14 species	34 reactions
8	Li-2015 [86]	14 species	37 reactions
9	Starik-2009 [87]	16 species	44 reactions
10	GRI3.0-1999 [88]	15 species (obtained from an original number of 53)	48 reactions (obtained from an original number of 325)
11	Rasmussen-2008 [89]	15 species (obtained from an original number of 24)	59 reactions (obtained from an original number of 105)
12	SaxenaWilliams-2006 [78]	14 species	30 reactions
13	Sun-2007 [90]	15 species	48 reactions
14	Ahmed-2007 [91]	14 species (obtained from an original number of 246)	37 reactions (obtained from an original number of 1284)
15	Zsély-2005 [49]	13 species	44 reactions
16	Dagaut-2003 [92]	13 species (obtained from an original number of 132)	34 reactions (obtained from an original number of 922)

An interesting comparison of the different kinetic schemes that have been developed for syngas combustion in gas turbines is proposed in the work of Olm et al. [79]. Sixteen combustion mechanisms for syngas are compared, based on the performances on 5 parameters:

– ignition delay;

– flame velocities;

– species concentrations;

– overall results, all diluents except He;

– overall results, all diluents including He.

To evaluate the performance on the 5 parameters an error function is considered, which is calculated in the following way:

$$E_i = \frac{1}{N_i} \sum_{j=1}^{N_i} \left(\frac{Y_{ij}^{\text{sim}} - Y_{ij}^{\text{exp}}}{\sigma \left(Y_{ij}^{exp} \right)} \right)^2 \tag{12.14}$$

where,

– N is the number of available data.

– Y_{ij}^{sim} is the j-th simulated data;

– Y_{ij}^{exp} is the j-th experimental data;

– $\sigma(Y_{ij}^{\text{exp}})$ is the standard deviation of the j-th experimental data.

The total error is the sum of the errors obtained from Eq. (12.15):

$$E = \frac{1}{N_i} \sum_{j=1}^{N} E_i \tag{12.15}$$

The mechanisms are assigned a number based on their performance on the 5 chosen parameters (number 1 is the best, number 16 is the worst), they are shown in Table 12.4.

Here the model used to simulate CO/H_2 mixtures by the CRECK modeling group is shown. This model is the first step in the implementation of the CRECK-2012 model and contains a large number of the reactions. We chose to present this model given the experience on biomass modeling of the CRECK research group. This model has been realized by adding the hydrogen oxidation mechanism [76] to the oxidation of CO. In this way the model is mainly based on the oxidation of H_2/CO mixtures, where CO and H_2 are the main components of syngas.

The model has been verified by comparing the results with experimental data obtained mainly under high-pressure conditions. It is thought to be used to model syngas combustion in gas turbines in a wide range of conditions. The kinetic model includes:

– recent and accurate thermodynamic and kinetic estimates;

– the interaction of the combustion system with pollutant species (NO_x) [93].

The scheme published in [74], which is based on 32 elementary reactions is proposed in Table 12.5. The part on methane combustion is taken from Ranzi et al. [94].

Table 12.5

$CO/H_2/O_2$ mechanism with rate coefficients in the form k = A · T n · exp(−Ea/RT), A units: mol/l/s/K; E_a units: cal/mol [74]

	Reaction	A	n	E[a]	Source
1	H+ O_2 = OH + O	2.21E+11	0	16,650	[76]
2	O+ H_2 = OH + H	4.33E+10	0	10,000	[76]
3	H+ O_2 + [M] = HO_2 + [M]	4.65E+09	−0.8	0	[76]
Low-pressure limit:		7.00E + 11	0.4	0	
Troe parameters: 0.5, 1E − 30 1E + 30					
Enhanced third-body efficiencies: H_2O = 18.0, H_2 = 2.5, N_2 = 1.26, O_2 = 0, Ar = 0.8, He = 0.8, CO = 1.2, CO_2 = 2.4					
	H + O_2 + O_2 = HO_2 + O2	8.90E+0.8	0	−2822	[76]
4	OH+ HO2 = H2O + O2	5.00E+10	0	1000	[76]
5	H+ HO_2 = OH + OH	2.50E+11	0	1900	[76]
6	O+ HO_2 = O_2 + OH	3.25E+10	0	0	[76]
7	OH + OH=O + H_2O	7.36E+09	0	1100	[76]
8	H_2 + [M] = H + H+[M]	2.23E+11	0	96,081	[76]
Enhanced third-body efficiencies: H_2O = 12.0, H_2 = 2.5, CO = 1.9, CO_2 = 3.8, Ar = 0.5, He = 0.5					
9	O_2 + [M] = O + O+[M]	1.55E+11	0	115,120	[76]
Enhanced third-body efficiencies: H_2O = 12.0, H_2 = 2.5, CO = 1.9, CO_2 = 3.8, Ar = 0.2, He = 0.2					
10	H + OH+[M] + H_2O+[M]	4.502E+16	−2	0	[76]
Enhanced third-body efficiencies: H_2O = 16.0, H_2 = 2.0, CO_2 = 1.9					
11	H + HO_2 = H_2 + O_2	2.50E+10	0	700	[76]
12	HO_2 + HO_2 = H_2O_2 + O_2	2.11E+09	0	0	[76]
13	OH + OH+[M] = H_2O_2 + [M]	7.40E+10	−0.37	0	[76]

	Reaction	A	n	E^a	Source
Low-pressure limit:		2.30E + 12	−0.9	−1700	
Troe parameters: 0.7346, 94.00, 1756, 5182					
Enhanced third-body efficiencies: H_2O = 6, H_2 = 2, CO = 1.5, CO_2 = 2.0, CH_4 = 2.0, C_2H_6 = 3.0, Ar = 0.7, He = 0.7					
14	O + OH+[M] = HO_2 + [M]	1.00E+10	0	0	[76]
15	H + H_2O=H_2 + OH	4.00E+07	1	19,000	[76]
16	H_2O_2 + H=H_2O + OH	2.41E+10	0	3970	[76]
17	H_2O_2 + H=H_2 + HO_2	6.03E+10	0	7950	[76]
18	HO_2 + H_2O → H_2O_2 + OH	5.39E+05	2	28,780	[76]
19	OH + H_2O_2 → H_2O + HO_2	3.20 + E+05	2	−4170	[76]
20	O + H_2O_2 → OH + HO_2	1.08E+06	2	−1657	[95]
21	CO + O+[M] = CO2 + [M]	9.64E+07	0	3800	[48]
Low-pressure limit:		2.07E + 20	−3.34	7610	
Enhanced third-body efficiencies: H2O = 12.0, H2 = 2.0, CO = 1.5, CO2 = 2.0, Ar = 0.5					
22	CO + OH=CO_2 + H	9.60 + 08	0.14	7352	
23	CO + H_2O=CO_2 + OH	3.01E+10	0	23,000	[47]
24	CO + H_2O=CO_2 + H_2	2.00E+08	0	38,000	[95]
25	O_2 + CO=CO_2 + O	2.53E+09	0	47,000	[96]
26	HCO+[M] = CO + H+[M]	1.20E+14	−1	17,000	[97]
Enhanced third-body efficiencies: H_2O = 5.0, H2 = 1.9, CO = 1.9, CO_2 = 3.0					
27	HCO + O=CO_2 + H	3.00E+10	0	0	[96]
28	HCO + H=H_2 + CO	1.00E+11	0	0	[98]
29	HCO + OH=H_2O + CO	5.00E+10	0	0	[99]
30	HCO + HO_2 = H_2O_2 + CO	4.00E+08	0	0	[94]
31	O_2 + HCO=H_2O + CO	1.00E+09	0	0	[94]
32	HCO + HO_2= > H + OH + CO_2	3.00E+10	0	0	[99]

The first reaction consists on the oxidation of a single hydrogen atom, which is a chain branching reaction, where O is a diradical; so in this step from one H radical 3 radical products are formed. The diradical can react with a hydrogen molecule to form two radicals (see branching reaction number 2). The two branching reactions can be responsible of explosion phenomena.

$$H + O_2 = OH + O \tag{12.16}$$

$$O + H_2 = OH + H \tag{12.17}$$

The third-order reaction, $H + O_2 + M = HO_2 + M$, is important as a chain terminating reaction in combustion. The reaction competes with the branching reaction, $H + O_2 = OH + O$, at temperatures less than ~900 K and, therefore, has a substantial effect in the later stages of combustion in both flames and practical combustors [100, 101].

$$H + O_2 + [M] = HO_2 + [M] \tag{12.18}$$

Equation (12.18) can involve also a H radical and two molecules of oxygen ($H + O_2 + O_2 = HO_2 + O_2$).

The reaction $OH + HO_2 = H_2O + O_2$ (shown in Eq. 12.19) plays an important role in combustion chemistry. It is a major HO_2 termination path in lean combustion [102, 103], and it is responsible for the depletion of both OH and HO_2 radicals in burnt gases [104, 105].

$$OH + HO_2 = H_2O + O_2 \tag{12.19}$$

The H_2/CO_2 sub-mechanism consists of 20 reversible reactions, as reported in [76]. The extension to syngas combustion requires the addition of only three new species (CO, CO_2 and HCO) and 12 new reactions.

As reported in the work of Davis [48], the reaction $CO + OH = CO_2 + H$ is the critical step in syngas oxidation and combustion and special attention should be focused on its rate constant. The importance of this reaction in syngas combustion is linked with the significant heat released during CO to CO_2 conversion. This reaction has been experimentally studied by Wooldridge et al. [106] who suggested a new expression to define the rate coefficient, based on experimental measures performed with infrared absorption of CO_2 and the UV laser absorption of OH. This rate is confirmed also by other measures reported in the literature [107, 108].

Davis et al. [48] added two modified Arrhenius expressions to describe more accurately the high temperature data of Wooldridge et al. [109] and of Golden et al. [110]. Similarly, a combination of two expressions was used by Joshi and Wang [108] while three expressions were combined by Sun et al. [111].

This is due to the complexity of the CO + OH reactions and to the difficulty in describing them using a single Arrhenius expression which should perform well over a wide range of temperatures. The

CO + OH reactions can proceed in both ways: passing and not passing through the chemically activated complex HOCO [108]. Consequently, the temperature dependence of the reaction can be explained better using two rate expressions and a two-channel reaction.

CO to CO_2 conversion can also proceed through the following recombination reaction:

$$\mathrm{CO} + \mathrm{O} + \mathrm{M} = \mathrm{CO_2} + \mathrm{M} \tag{12.20}$$

This happens mainly at high pressures and/or in anhydrous systems, as reported by [74]. Figure 12.18 shows that in literature we can find very different values of rate constants [47, 96, 112, 113, 114, 115, 116, 117, 118, 119]. In the model presented in Table 12.5 we can see that the reaction number 21 is modelled with the following Arrhenius expression:

$$k = 2.07 \times 1020 \times T - 3.34 \times \exp(-7160/\mathrm{RT}) \ \left[\mathrm{m^6/kmol^2/s}\right] \tag{12.21}$$

Fig. 12.18

Reaction CO + O + M = CO_2 + M. Comparison of the low-pressure rate constants suggested by [47, 74, 96, 112, 113, 114, 115, 116, 117, 118, 119] (K units: mol cm^3 s). Reprinted with permission from [74]. Copyright © 2007, Elsevier

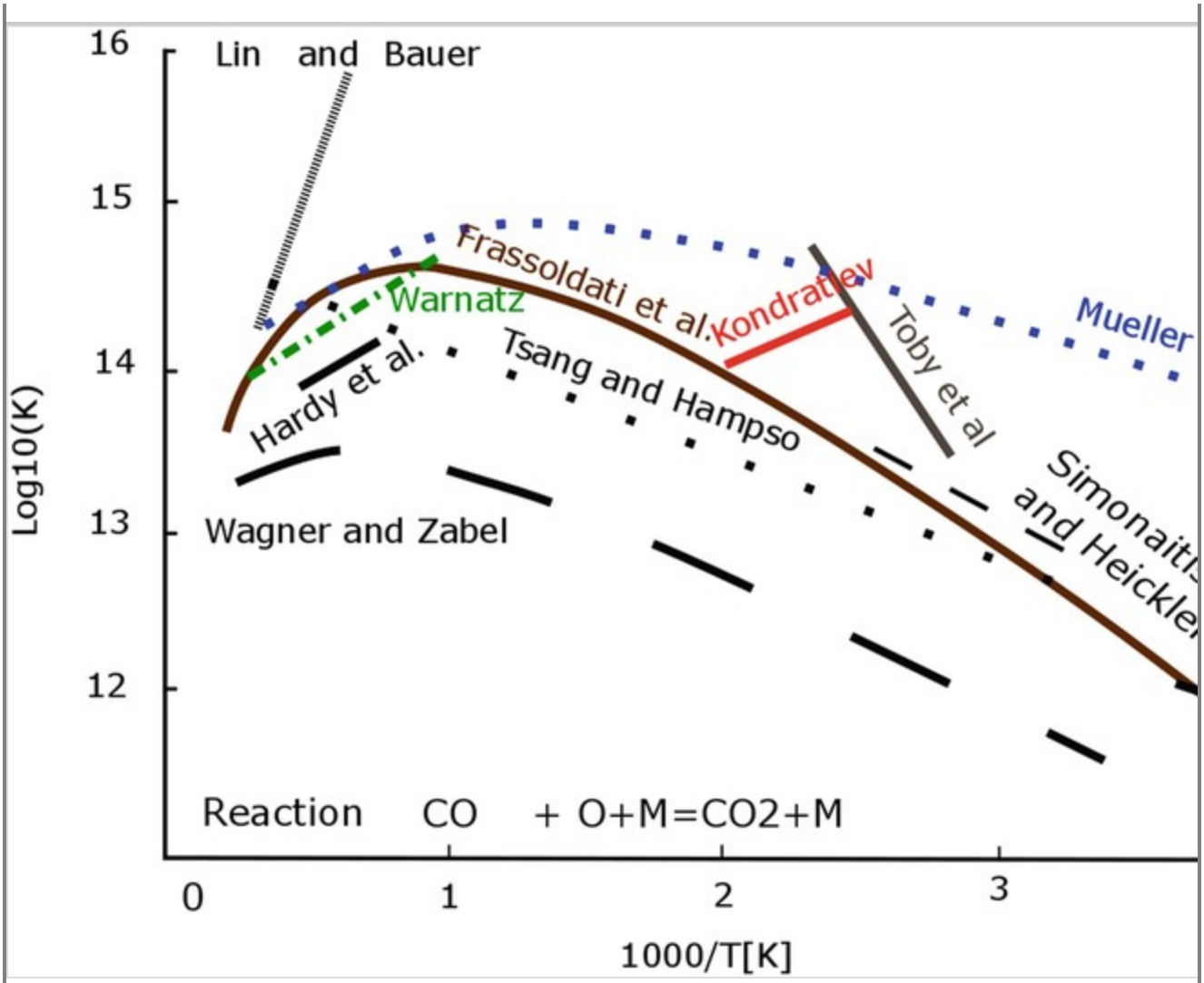

Which in case of high-pressure is combined with the parameters of Kondratiev [120] as suggested by Allen et al. [121]. The value of the kinetic rate at high-pressure value is about 2–3 times faster than the one suggested by Troe [122]. Dealing with the reaction, Eq. (12.22),

$$CO + HO_2 = CO_2 + OH \qquad 12.22$$

the equation was modified, according to what reported in Mueller et al. [47], to take into account of syngas reactivity at low temperature and high pressure.

Nitrogen chemistry and kinetics has been analyzed in many papers [76, 123, 124]. The kinetic model presented in Table 12.5 can be combined with a NO_x kinetic scheme in which the following reaction was updated to improve the model predictions:

$$HONO + OH = NO_2 + H_2O \qquad 12.23$$

AQ5

Another interesting scheme, which is not comprised in Table 12.5 is the one proposed by Boivin *et al* [125]. This is a four step mechanism which builds upon a three step mechanism for H_2 combustion in air [126]. Also in this case CO combustion is added to an already existing scheme describing H_2 combustion. The final scheme is quite simple and composed by 16 elementary steps.

12.4.2. Experimental Pressurized Syngas Combustion Test Benches

Burke et al.[127] have used a dual-chambered, pressure-release type high-pressure combustion apparatus (see Fig. 12.19) to assess the influence of temperature and pressure on mass burning rates of syngas with different compositions.

Fig. 12.19

Dual chamber high pressure combustion apparatus. Reprinted with permission from [127]. Copyright © 2010, Elsevier

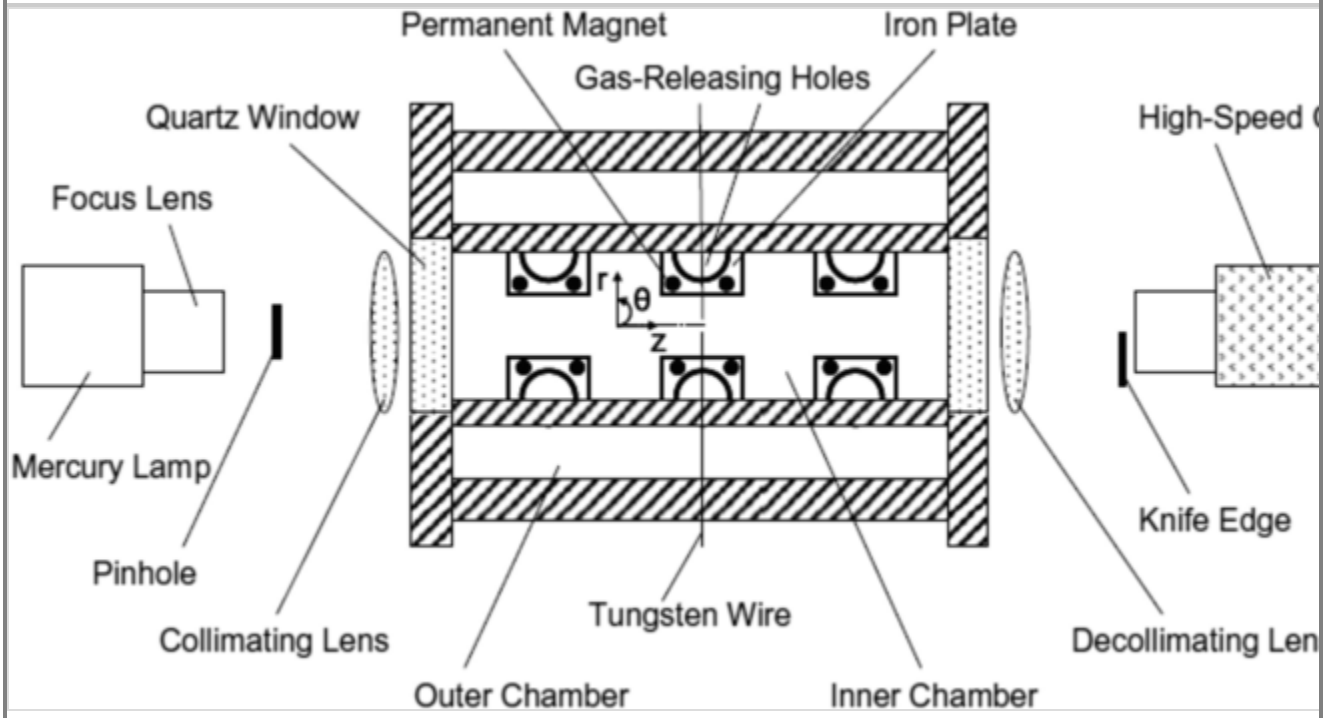

In recent studies, the facility shown in Fig. 12.19 was managed in the “closed configuration”, as discussed in [128], such that the combustion chamber can be considered as a constant-volume cylindrical bomb. Experimentally and numerically studies have been done to investigate the dependences between the pressure and flame temperature of mass burning rates for H_2/CO/O_2/diluents blends. Mass burning rates and flame speeds were extracted from externally propagating flames for equivalence ratios from 0.85 to 2.5, flame temperatures of (1500–1800) K, pressures from (1 to 25) atm, CO fuel fractions from 0 to 0.9 and dilution concentrations of He, Ar and CO_2 up to respectively 0.8, 0.6 and 0.4. The main conclusions are explained in the following paragraphs:

At low pressure, the mass burning rate increases with pressure, while at high pressure conditions there is an inversely proportional relationship between the mass burning rate and the pressure for both lean and rich conditions. A negative dependence of the mass burning rate on pressures is observed at lower pressure and lower temperature. With the increase of pressure the dependence on temperature of the burning rate increases. Compared to pure H_2 at the same pressure and temperature conditions, 0.5 fraction of carbon monoxide addition to the fuel doesn't have an important effect on the pressure dependence. Dilution with CO2 enhances the pressure and temperature dependence.

Currently there is no kinetic model which can predict the dependence of the burning rate on pressure across all the pressure and temperature conditions.

Dealing with experiments which applied the typical conditions of a gas turbine combustion chamber in an IGCC. In order to keep the same flame temperature, the dilution can be increased together with the preheating of the mixture; this will give the same burning rate-pressure dependence with respect to the non-preheated test. Burning rate-pressure dependence and sensitivity results are reduced in the case of preheating the mixture with fixed dilution rates. Referring to the previous case, if dilution is not maintained constant, but it is decreased then we will have also an increase in the flame temperature and a weaker dependence of burning rate from pressure. The strength of the burning rate-pressure dependence of H_2/O_2/diluent flames is influenced by diluent according to the following order: $He < N_2 < CO_2 < H_2O$.

When the pressure is increased, the extended second explosion limit, which delimits straight-chain kinetics from chain-branching kinetics, translates to higher temperatures. As a result, the part of the flame zone in which intense branching happens is restricted to a narrower, higher temperature window as the pressure is increased—resulting in a shift of the peak for all radical reactions to higher temperatures. According to the sensitivity analysis, the pressure dependence for rich conditions is controlled by two competing chemical reactions:

- $H + O_2$.
- and $H + HO_2$.

which largely govern the fate of H. The same reactions are important for lean conditions together with:

- $OH + H_2$.
- and $OH + HO_2$.

which are mainly responsible of the OH radical fate.

The sensitivity of mass burning rates to elementary rate constants increases greatly with pressure. The big sensitivities at elevated pressures raise the effects of uncertainties in rate constants for elementary reactions. Consequently, the inconsistencies in the burning rate predictions by different models may be due to uncertainties associated with a number of reactions, radical recombination reactions; such as HO_2 + radical reactions, radical recombination reactions and even well-studied reactions (like hydrogen oxidation reactions). The collision efficiencies, as well as the treatment of fall off for the

reaction: $H + O_2(+M) = HO_2(+M)$ can influence in an important way the predictions at high pressures, whereas for “fall off” a reaction has an increasing rate with an increase in temperature.

It becomes clear that one or more elementary reactions could be significant in high-pressure H_2 flames but are not considered by the most part of the current H_2 combustion models (eg. $O + OH + M = HO_2 + M$).

In the case of increasing pressure and decreasing flame temperature, the recombination reactions are thought to become more important. For this reason the flux through branching and recombination channels may become approximately equal in the most reactive portion of the flame at low flame temperatures and high pressures conditions. Hence, the sensitivity of the predictions to the rate parameters for those reactions increase dramatically. The high sensitivities to input parameters important implications. For example it will be very difficult to model exactly the flame at high-pressure an uncertainty in a rate parameter will results in a larger uncertainty in the flame speed/burning rate.

Another experimental apparatus is shown in Fig. 12.20; this has been realized in the ‘Centro Combustione Ambiente’ Gioa del Colle, through the collaboration of Ansaldo and Turbec, it is based on a pressurized combustion chamber which simulated the combustion chamber of a micro-gasturbine. Tests have been performed to understand the combustor performances when fed with compressed air from bottles and a mixture of syngas and steam; where syngas is provided by bottles.

Fig. 12.20

Simplified overview of the experimental setup used to test different fuel types in the pressurized combustor. Reprinted with permission from [129]. Copyright © 2010, Elsevier

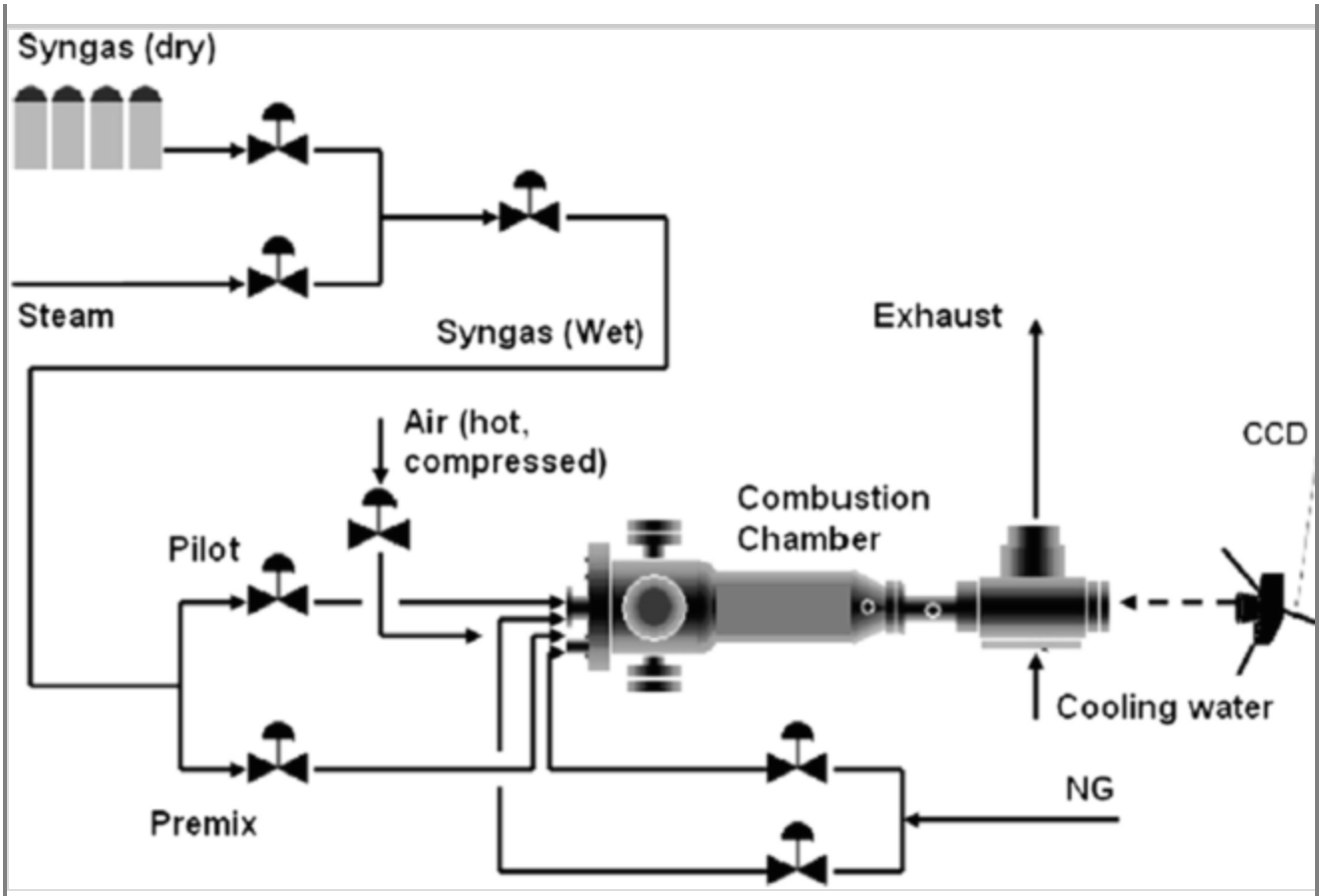

Figure 12.20 shows a clarified view of the experimental installation used to fire the pressurized combustion on NG/syngas or a mixture of both. The flows of compressed carbon monoxide (20.5 vol.%) and hydrogen (79.5 vol.%) are regulated via electronic valves. The steam is generated externally and premixed to create a wet syngas. The temperature of the combustion mixture is monitored using 24 K type thermocouples. Pressure sensors are used to monitor the pressure ratio of the air when it is compressed externally to the combustion chamber. Downstream of the combustion chamber, there is a diaphragm that regulates the pressure and represents the turbine backpressure. Electric heaters preheat the air up to a theoretical maximum of 450 °C. To maintain the same pressure drop used for methane the injection nozzles were slightly to optimize the injection of hydrogen-rich synthesis gas.

The combustion gases are cooled by a water-cooling circuit respectively after passing the adjustable diaphragm and before being analyzed to determine their composition and evacuated through the exhaust pipe.

After the syngas combustion tests in a microturbine combustion chamber, it can be inferred that:

- the values obtained during measurements of wall-temperature for the combustion of synthesis gas did not exceed those obtained with natural gas. So there should be no problem regarding temperature limits of the materials due to the use of wet hydrogen-rich gas.

- during partial load and full load operation of the syngas combustion chamber, no observations have been made which could indicate a declining flame anchoring position. According to the

temperature profiles, it can be noted that the flame does not come close to the combustor rim, so there are not flashback problems.

- the production of NO_x and CO measured over combustion remain notably low. It can be note that the combustion regime was stable producing very low CO emissions during the operation with syngas. So no incomplete combustion was observed. The small values for the NOx emissions are due to the positive effect of the steam content on flame temperature. So thermal NOx have been minimized. Prompt NO_x was not awaited to have significant contributions. Correspondingly, the total NO_x emissions generated during syngas combustion were found to be with a very small value, under (<5 ppm).

- no auto-ignition, flashback instabilities or blow-off were noticed.

12.5. Conclusions and Future Outlook

Syngas is the product of pyrolysis and gasification processes which can be used both for CHP and for the production of chemicals. Syngas compression is a useful process which can boost its utilization in many cases: for the chemical conversion of the gas; for power production in IGCC plants; for heat production for cooking and heating needs. The compression has to be performed in safe and effective ways. This chapter shows that:

- it is important to analyze the explosion limit of the syngas, the ignition delay and the behavior of syngas in high pressure and high temperature environments.

- this can be done following two approaches: experimental and modeling.

- experiments can be performed in Rapid Compression Facility (RCM) test bench and also I shock tube reactors.

- kinetic models can be verified on experimental data and used to simulate syngas behavior and the combustion performances of gases with different composition which are compressed and ignited in different conditions of temperature and pressure.

- experimental tests have shown that after ignition the pressure data show an increase, which is slow at first and then is followed by a rapid increase.

- further studies have shown as auto-ignition can be of two types: strong and weak. Weak ignition is defined as non-uniform ignition of the mixture; while strong ignition is defined as a phenomenon which starts with a wave that propagates through all the combustible mixture. The weak ignition can be explained with a kinetic phenomenon which is delimited by the second explosion limit.

- weak ignition is a phenomenon linked with the dynamics of the gases and it is induced by perturbations to the flow-field. It has to be taken into consideration also that the strong ignition is located usually at temperatures which are higher than 1000 K. The strong ignition limit is not existent anymore at high pressures, where it has been assessed only strong ignition (i.e homogeneous ignition).

- when the pressure is increased, the extended second explosion limit, which delimits straight-chain kinetics from chain-branching kinetics, translates to higher temperatures. As a result, the part of the flame zone in which intense branching happens is restricted to a narrower, higher temperature window as the pressure is increased – resulting in a shift of the peak for all radical reactions to higher temperatures.

- according to sensitivity analysis, the pressure dependence for rich conditions is controlled by two competing chemical reactions: $H + O_2$ and $H + HO_2$; which largely govern the fate of H. The same reactions are important for lean conditions together with: $OH + H_2$ and $OH + HO_2$; which are mainly responsible of the OH radical fate.

Dealing with future outlook and future areas of research, if the syngas has to be compressed and stored in closed vessels, the condensation of tar will be very in the compressed syngas systems as this is a new topic which deserves to be better studied to protect the components of the compressor and ensure the long life of the process. For this aspect, modeling of tar dew point will be of paramount importance in the design and optimization. Systems will be needed to:

- extract the condensed tar from the compressor;

- avoid tar entering the compressor itself;

- model tar dew point and tar condensation.

References

1. D'Alessandro B, D'Amico M, Desideri U, Francesco F. The IPRP (integrated pyrolysis regenerated plant) technology: from concept to demonstration. Appl Energy. 2013;101(1):423–31. https://doi.org/10.1016/j.apenergy.2012.04.036.

2. Zhang X, Che Q, Cui X, Wei Z, Zhang X, Chen Y, Wang X, Chen H. Application of biomass pyrolytic polygeneration by a moving bed: characteristics of products and energy efficiency analysis. Bioresour Technol. 2018;254:130–8. https://doi.org/10.1016/j.biortech.2018.01.083.

3. Minchener AJ. Coal gasification for advanced power generation. Fuel. 2005;84(17):2222–35. https://doi.org/10.1016/j.fuel.2005.08.035.

4. Beaudin M, Zareipour H, Schellenberglabe A, Rosehart W. Energy storage for mitigating the variability of renewable electricity sources: an updated review. Energy Sustain Dev. 2010;14(4):302–14. https://doi.org/10.1016/j.esd.2010.09.007.

5. Tukiainen S. Carbofex EBC-certified biochar technology, Carbofex. 2020. https://www.carbofex.fi/. Accessed 18 Jan 2020.

6. Carbon Terra. Das unternehmen. 2020. https://www.carbon-terra.eu/en/schottdorf-meiler/functionality. Accessed 18 Jan 2020.

7. Gustafsson M. 2013Pyrolysis for heat production. Master thesis. 2013. http://www.diva-portal.org/smash/get/diva2:655188/FULLTEXT02.pdf. Accessed 18 Jan 2020.

8. EliquoStulz. PYREG, Minimise the cost of your sludge disposal. 2020. https://www.eliquostulz.com/en/pyreg.html. Accessed 18 Jan 2020.

9. Ahmad E, Jäger N, Apfelbacher A, Daschner R, Hornung A, Pant KK. Integrated thermo-catalytic reforming of residual sugarcane bagasse in a laboratory scale reactor. Fuel Process Technol. 2018;171:277–86. https://doi.org/10.1016/j.fuproc.2017.11.020.

10. 3R Agrocarbon. The 3R zero emission pyrolysis technology generates new resources and added value recovered BIO-PHOSPHATE products. 2020. https://www.3ragrocarbon.com/sites/default/files/attachments/3r_fact_sheet.pdf. Accessed 18 Jan 2020

11. Rietveld G, van der Drift A, Grootjes AJ, van der Meijden CM, Vreugdenhil BJ. Commercialization of the ECN MILENA gasification technology, ECN report ECN-M--14-061. 2014. https://publications.tno.nl/publication/34631595/N4tX73/m14061.pdf. Accessed 18 Jan 2020.

12. Ahrenfeldt J, Thomsen TP, Henriksen U, Clausen LR. Biomass gasification cogeneration – a review of state of the art technology and near future perspectives. Appl Therm Eng. 2013;50(2):1407–17. https://doi.org/10.1016/j.applthermaleng.2011.12.040.

13. Hofbauer H, Rauch R, Bosch K, Koch R, Aichernig C. Biomass CHP plant güssing - a success story. 2002. https://www.semanticscholar.org/paper/Biomass-CHP-Plant-G%C3%BCssing-A-Success-Story-Hermann-Reinhard/0122da66ae2088ad3f046a150f251a4a345b8038. Accessed 18 Jan 2020.

14. Biollaz S. The SNG technology platform in güssing, a status report of bio-SNG project. In: Poster presented at European Biofuels Technology Platform: Second Stakeholder Plenary Meeting (SPM2), 22nd of January 2009, Brussels. 2009. http://www.etipbioenergy.eu/images/Poster_BioSNG_PSI.pdf. Accessed 18 Jan 2020.

15. Alamia A, Magnusson I, Johnsson F, Thunman H. Well-to-wheel analysis of bio-methane via gasification, in heavy duty engines within the transport sector of the European Union. Appl Energy. 2016;170:445–54. https://doi.org/10.1016/j.apenergy.2016.02.001.

16. Hedenskog M. The GoBiGas project: bio-methane from forest residues – from vision to reality. Presentation at SVEBIO2015. 2015.

17. Alamia A, Larsson A, Breitholtz C, Thunman H. Performance of large-scale biomass gasifiers in a biorefinery, a state-of-the-art reference. Int J Energy Res. 2017;41:2001–19. https://doi.org/10.1002/er.3758.

18. Larsson A, Hedenskog M, Thunman H. Monitoring the bed material activation in the GoBiGas-Gasifier. In: Nordic Flame days. 2015. https://www.researchgate.net/publication/283578378_Monitoring_the_Bed_Material_Activation_in_the_GoBiGas-Gasifier. Accessed 18 Jan 2020.

19. Rauch R, Hofbauer H, Bosch K, Siefert I, Aichernig C, Voigtlaender K et al. Steam gasification of biomass at CHP plant guessing-status of the demonstration plant. In: World biomass conference; biomass for energy industry and climate protection, pp 1687–1690. 2004.

20. Pfeifer C, Koppatz S, Hofbauer H. Steam gasification of various feedstocks at a dual fluidised bed gasifier: impacts of operation conditions and bed materials. Biomass Convers Biorefin. 2011;1:39–53. https://doi.org/10.1007/s13399-011-0007-1.

21. Kotik J. Über den Einsatz von Kraft-Wärme-Kopplungsanlagen auf basis der wirbelschichtdampfvergasung fester biomasse am beispiel des biomassekraftwerks oberwart. Vienna: Vienna University of Technology; 2010.. (in German)

22. Suda T, Liu Z, Takafuji M, Hamada K, Tani H. Gasification of lignite coal and biomass using twin IHI Gasifier (TIGAR®). 2012. https://www.ihi.co.jp/var/ezwebin_site/storage/original/application/fae45aac0eb82bef2ca20cf8cc2cb0f0.pdf. Accessed 18 Jan 2020.

23. Paethanom A. Twin IHI Gasifier (TIGAR®) – current status of Indonesian demonstration project and its business plan. In gasification and syngas technologies conference. Vancouver, BC. 2016. https://www.globalsyngas.org/members/2016-conference-presentations/. Accessed 18 Jan 2020.

24. Melligan F, Auccaise R, Novotny EH, Leahy JJ, Hayes MHB, Kwapinski W. Pressurised pyrolysis of Miscanthus using a fixed bed reactor. Bioresour Technol. 2011;102(3):3466–70. https://doi.org/10.1016/j.biortech.2010.10.129.

25. Mahinpey N, Murugan P, Mani T, Raina R. Analysis of bio-oil, biogas, and biochar from pressurized pyrolysis of wheat straw using a tubular reactor. Energy Fuel. 2009;23:2736–42. https://doi.org/10.1021/ef8010959.

26. Fjellerup J, Gjernes E, Hansen LK. Pyrolysis and combustion of pulverized wheat straw in a pressurized entrained flow reactor. Energy Fuel. 1996;10:649–51. https://doi.org/10.1021/ef950204e.

27. Whitty K, Backman R, Hupa M. Influence of pressure on pyrolysis of black liquor: 1. Swelling. Bioresour Technol. 2008;99:663–70. https://doi.org/10.1016/j.biortech.2006.11.065.

28. Roberts DG, Harris DJ, Wall TF. On the effects of high pressure and heating rate during coal pyrolysis on char gasification reactivity. Energy Fuel. 2003;17:887–95. https://doi.org/10.1021/ef020199w.

29. Matsuoka K, Akiho H, Xu WC, Gupta R, Wall TF, Tomita A. The physical character of coal char formed during rapid pyrolysis at high pressure. Fuel. 2005;84:63–9. https://doi.org/10.1016/j.fuel.2004.07.006.

30. Vuthaluru HB. Investigations into the pyrolytic behaviour of coal/biomass blends using thermogravimetric analysis. Bioresour Technol. 2004;92:187–95. https://doi.org/10.1016/j.biortech.2003.08.008.

31.

Cetin E, Gupta R, Moghtaderi B. Effect of pyrolysis pressure and heating rate on radiata pine char structure and apparent gasification reactivity. Fuel. 2005;84:1328–34. https://doi.org/10.1016/j.fuel.2004.07.016.

32. Porada S. The influence of elevated pressure on the kinetics of evolution of selected gaseous products during coal pyrolysis. Fuel. 2004;83(7–8):1071–8. https://doi.org/10.1016/j.fuel.2003.11.004.

33. Blackmer®. Compressors, 04/99 CB-207. 2020. https://www.gasequipment.com/catalogs/cryogenic/pdf/Blackmer/Compressors/Comp%20Selection%20and%20Sizing.pdf. Accessed on 17 Jan 2020.

34. Process Industry Practices Machinery. Compressor selection guidelines. 2013. https://pip.org/docs/default-source/practices-documents/reec001bf1ca80395a262f789edff00008ddc6a.pdf?sfvrsn=d3beca9e_0. Accessed 17 Jan 2020.

35. Gresh MT. Compressor performance: aerodynamics for the user. Amsterdam: Elsevier; 2001.

36. Rezvani S, McIlveen-Wright D, Huang Y, Dave A, Deb Mondol J, Hewitt N. Comparative analysis of energy storage options in connection with coal fired integrated gasification combined cycles for an optimized part load operation. Energy Convers Manag. 2012;101:154–60. https://doi.org/10.1016/j.fuel.2011.07.034.

37. Amos WA. Costs of storing and transporting hydrogen. National Renewable Energy Lab, Golden, CO. 1999. https://www.nrel.gov/docs/fy99osti/25106.pdf. Accessed 17 Jan 2020.

38. Cau G, Cocco D, Serra F. Energy and cost analysis of small-size integrated coal gasification and syngas storage power plants. Energy Convers Manag. 2012;56:121–9. https://doi.org/10.1016/j.enconman.2011.11.025.

39. Richards GA, McMillian MM, Gemmen RS, Rogers WA, Cully SR. Issues for low-emission, fuel-flexible power systems. Prog Energy Combust Sci. 2001;27(2):141–69. https://doi.org/10.1016/S0360-1285(00)00019-8.

40. Lieuwen T, McDonell V, Santavicca D, Sattelmayer T. Burner development and operability issues associated with steady flowing syngas fired combustors. Combust Sci Technol. 2008;180(6):1169–92. https://doi.org/10.1080/00102200801963375.

41. He F, Li Z, Liu P, Ma L, Pistikopoulos EN. Operation window and part-load performance study of a syngas fired gas turbine. Appl Energy. 2012;89(1):133–41. https://doi.org/10.1016/j.apenergy.2010.11.044.

42. Frey HC, Zhu Y. Improved system integration for integrated gasification combined cycle (IGCC) systems. Environ Sci Technol. 2006;40:1693–9. https://doi.org/10.1021/es0515598.

43. Smith AR, Klosek J. A review of air separation technologies and their integration with energy conversion processes. Fuel Process Technol. 2001;70(2):115–34. https://doi.org/10.1016/S0378-3820(01)00131-X.

44. Geosits RF, Schmoe Lee A. IGCC – the challenges of integration. In: Proceedings of GT2005 ASME turbo expo 2005: power for land, sea, and air, Reno, NV. 2005. https://www.edockets.state.mn.us/EFiling/edockets/searchDocuments.do?method=showPoup&documentId={1AB68706-28A0-4706-B9A8-5C412EAF4BDE}&documentTitle=281454. Accessed 17 Jan 2020.

45. Jaeger H. Plant design net rated 644 MW and 38% HHV on low rank coal, gas turbine world; March–April 2006. 2006.

46. Lee C, Lee SJ, Yun Y. Effect of air separation unit integration on integrated gasification combined cycle performance and NOx emission characteristics. Korean J Chem Eng. 2007;24(2):368–73. https://doi.org/10.1007/s11814-007-5047-7.

47. NATO. Performance prediction and simulation of gas turbine engine operation for aircraft, marine, vehicular, and power generation. Technical report RTO-TRAVT-036. Research and Technology Organisation, North Atlantic Treaty Organisation. 2007. https://apps.dtic.mil/docs/citations/ADA466188. Accessed 17 Jan 2020.

48. Gupta KK, Rehman A, Sarviya RM. Bio-fuels for the gas turbine: a review. Renew Sustain Energy Rev. 2010;14(9):2946–55. https://doi.org/10.1016/j.rser.2010.07.025. Accessed 17 Jan 2020

49. Todd DM, Battista RA. Demonstrated applicability of hydrogen fuel for gas turbines. In: Proceedings of gasification for the future, Noordwijk, Nederland. 2000.

50. Shilling N, Jones RM. The response of gas turbines to a CO2 constrained environment. In: Gasification technology conference report, GE Power Systems.

51. Chiesa P, Lozza G, Mazzocchi L. Using hydrogen as gas turbine fuel. Trans ASME J Eng Gas Turb Power. 2005;127(1):73–80. https://doi.org/10.1115/1.1787513.

52. Gardiner WC Jr, McFarland M, Morinaga K, Takeyama T, Walker BF. Initiation rate for shock-heated hydrogen-oxygen-carbon monoxide-argon mixtures as determined by OH induction time measurements. J Phys Chem. 1971;75:1504–9. https://doi.org/10.1021/j100680a022.

53. Dean AM, Steiner DL, Wang EE. A shock tube study of the $H_2/O_2/CO/Ar$ and $H_2/N_2O/CO/Ar$ systems: measurement of the rate constant for H + N2O = N2 + OH combust. Flame. 1978;32:73–83. https://doi.org/10.1016/0010-2180(78)90081-0.

54. Fotache CG, Tan Y, Sung CJ, Law CK. Ignition of $CO/H_2/N_2$ versus heated air in counterflow: experimental and modeling results. Combust Flame. 2000;120:417–26. https://doi.org/10.1016/S0010-2180(99)00098-X.

55. Wierzba I, Kilchyk V. Flammability limits of hydrogen–carbon monoxide mixtures at moderately elevated temperatures. Int J Hydrogen Energy. 2001;26:639–43. https://doi.org/10.1016/S0360-3199(00)00114-2.

56. Mueller MA, Yetter RA, Dryer FL. Flow reactor studies and kinetic modeling of the H_2/O_2/NOX and $CO/H_2O/O_2$/NOX reactions. Int J Chem Kinet. 1999;31:705–24. https://doi.org/10.1002/(SICI)1097-4601(1999)31:10<705::AID-JCK4>3.0.CO;2-%23.

57. Davis SG, Joshi AV, Wang H, Egolfopoulos F. An optimized kinetic model of H2/CO combustion. Proc Combust Inst. 2005;30:1283–92. https://doi.org/10.1016/j.proci.2004.08.252.

58. Zsely IG, Zador J, Turanyi T. Uncertainty analysis of updated hydrogenand carbon monoxide oxidation mechanisms. Proc Combust Inst. 2005;30:1273–81. https://doi.org/10.1016/j.proci.2004.08.172.

59. Walton SM, He X, Zigler BT, Wooldridge MS. An experimental investigation of the ignition properties of hydrogen and carbon monoxide mixtures for syngas turbine applications. Proc Combust Inst. 2007;31(2):3147–54. https://doi.org/10.1016/j.proci.2006.08.059.

60. Donovan MT, He X, Zigler BT, Palmer TR, Wooldridge MS, Atreya A. Demonstration of a free-piston rapid compression facility for the study of high temperature combustion phenomena. Combust Flame. 2004;137(3):351–65. https://doi.org/10.1016/j.combustflame.2004.02.006.

61. He X, Donovan MT, Zigler BT, Palmer TR, Walton SM, Wooldridge MS, Atreya A. Combust. Flame. 2005;142:266–75. https://doi.org/10.1016/j.combustflame.2005.02.014.

62. Lee D, Hochgreb S. Hydrogen autoignition at pressures above the second explosion limit (0.6–4.0 MPa). Int J Chem Kinet. 1998;30:385–406. https://doi.org/10.1002/(SICI)1097-4601(1998)30:6<385::AID-KIN1>3.0.CO;2-O.

63. Elsworth JE, Haskell WW, Read IA. Non-uniform ignition processes in rapid-compression machines combust. Flame. 1969;13(4):437–8. https://doi.org/10.1016/0010-2180(69)90115-1.

64. Vermeer DJ, Meyer JW, Oppenheim AK. Auto-ignition of hydrocarbons behind reflected shock waves combust. Flame. 1972;18(3):327–36. https://doi.org/10.1016/S0010-2180(72)80183-4.

65. Fieweger K, Blumenthal R, Adomeit G. Self-ignition of S.I. engine model fuels: a shock tube investigation at high pressure combust. Flame. 1997;109(4):599–619. https://doi.org/10.1016/S0010-2180(97)00049-7.

66. Walton SM, He X, Zigler BT, Wooldridge MS, Atreya A. Demonstration of distinct ignition regimes using high-speed digital imaging of Iso-octane mixtures. In: Proc. fourth joint meeting of the US Sections of the Combust. Inst. https://ci.confex.com/ci/2005/techprogram/P1498.HTM

67. Walton SM, He X, Zigler BT, Wooldridge MS, Atreya A. An experimental investigation of iso-octane ignition phenomena. Combust Flame. 2007;150(3):246–62. https://doi.org/10.1016/j.combustflame.2006.07.016.

68. Wang H. Private communication. 2005.

69.

Chaos M, Dryer FL. Syngas combustion kinetics and applications. Combust Sci Technol. 2008;180(6):1053–96. https://doi.org/10.1080/00102200801963011.

70. Grogan KP, Ihme M. Weak and strong ignition of hydrogen/oxygen mixtures in shock-tube systems. Proc Combust Inst. 2015;35(2):2181–9. https://doi.org/10.1016/j.proci.2014.07.074.

71. Voevodsky VV, Soloukhin RI. On the mechanism and explosion limits of hydrogen-oxygen chain self-ignition in shock waves. Proc Combust Inst. 1965;10(1):279–83. https://doi.org/10.1016/S0082-0784(65)80173-4.

72. Meyer J, Oppenheim A. On the shock-induced ignition of explosive gases. Symp Combust. 1971;13(1):1153–64. https://doi.org/10.1016/S0082-0784(71)80112-1.

73. Mansfield AB, Wooldridge MS. High-pressure low-temperature ignition behavior of syngas mixtures. Combust Flame. 2014;161(9):2242–51. https://doi.org/10.1016/j.combustflame.2014.03.001.

74. Frassoldati A, Faravelli T, Ranzi E. The ignition, combustion and flame structure of carbon monoxide/hydrogen mixtures. Note 1: detailed kinetic modeling of syngas combustion also in presence of nitrogen compounds. Int J Hydrog Energy. 2007;32(15):3471–85. https://doi.org/10.1016/j.ijhydene.2007.01.011.

75. Mittal G, Sung CJ, Yetter RA. Autoignition of H_2/CO at elevated pressures in a rapid compression machine. Int J Chem Kinet. 2006;38:516. https://doi.org/10.1002/kin.20180.

76. Frassoldati A, Faravelli T, Ranzi E. A wide range modeling study of NOx formation and nitrogen chemistry in hydrogen combustion. Int J Hydrogen Energy. 2006;31(15):2310–28. https://doi.org/10.1016/j.ijhydene.2006.02.014.

77. Kalitan DM, Petersen EL. Ignition and oxidation of lean CO/H2 fuel blends in air 41st AIAA/ASME/SAE/ASEE joint propulsion conference and exhibit, 10–13 July 2005, Tucson, Arizona (USA), paper 2005-3767. 2005. https://doi.org/10.2514/1.28123.

78. Saxena P, Williams FA. Testing a small detailed chemical-kinetic mechanism for the combustion of hydrogen and carbon monoxide. Combust Flame. 2006;145:316–23. https://doi.org/10.1016/j.combustflame.2005.10.004.

79. Olm C, Zsély IG, Varga T, Curran HJ, Turányi T. Comparison of the performance of several recent syngas combustion mechanisms. Combust Flame. 2015;162:1793–812. https://doi.org/10.1016/j.combustflame.2014.12.001.

80. Healy D, Kalitan DM, Aul CJ, Petersen EL, Bourque G, Curran HJ. Oxidation of C1−C5 alkane quinternary natural gas mixtures at high pressures. Energy Fuel. 2010;24:1521–8. https://doi.org/10.1021/ef9011005.

81. Kéromnès A, Metcalfe WK, Heufer KA, Donohoe N, Das AK, Sung CJ, Herzler J, Naumann C, Griebel P, Mathieu O, Krejci MC, Petersen EL, Pitz WJ, Curran HJ. An experimental and detailed

chemical kinetic modeling study of hydrogen and syngas mixture oxidation at elevated pressures. Combust Flame. 2013;160:995–1011. https://doi.org/10.1016/j.combustflame.2013.01.001.

82. Li J, Zhao Z, Kazakov A, Chaos M, Dryer FL, Scire JJJ. A comprehensive kinetic mechanism for CO, CH2 O, and CH 3 OH combustion. Int J Chem Kinet. 2007;39(3):109–36. https://doi.org/10.1002/kin.20218.

83. Wang H, You X, Joshi AV, Davis SG, Laskin A, Egolfopoulos F, Law CK. USC Mech version II. High-temperature combustion reaction model of H2/CO/C1-C4 compounds. http://ignis.usc.edu/USC_Mech_II.htm/. Accessed 17 Jan 2020.

84. Mechanical and Aerospace Engineering (Combustion Research), University of California at San Diego: Chemical-Kinetic Mechanisms for Combustion Applications, San Diego Mechanism, version 2014-02-17. http://combustion.ucsd.edu. Accessed 17 Jan 2020.

85. CRECK modeling Group Hydrogen/CO mechanism version 1212. http://creckmodeling.chem.polimi.it/kinetic.html/. Accessed 17 Jan 2020.

86. Li X, You X, Wu F, Law CK. Uncertainty analysis of the kinetic model prediction for high-pressure H_2/CO combustion. Proc Combust Inst. 2015;35(1):617–24. https://doi.org/10.1016/j.proci.2014.07.047.

87. Starik AM, Titova NS, Sharipov AS, Kozlov VE. Syngas oxidation mechanism. Combust. Explos. Shock Waves. 2010;46:491–506. https://doi.org/10.1007/s10573-010-0065-x.

88. Smith GP, Golden DM, Frenklach M, Moriary NW, Eiteneer B, Goldenberg M, Bowman CT, Hanson RK, Song S, Gardiner WC, Lissianski VV, Qin Z. GRI-Mech 3.0. http://combustion.berkeley.edu/gri-mech/version30/text30.html. Accessed 15 Nov 2019.

89. Rasmussen CL, Hansen J, Marshall P, Glarborg P. Experimental measurements and kinetic modeling of CO/H_2/O_2/NOx conversion at high pressure. Int J Chem Kinet. 2008;40:454–80. https://doi.org/10.1002/kin.20327.

90. Sun H, Yang SI, Jomaas G, Law CK. High-pressure laminar flame speeds and kinetic modeling of carbon monoxide/hydrogen combustion. Proc Combust Inst. 2007;31(1):439–46. https://doi.org/10.1016/j.proci.2006.07.193.

91. Ahmed SS, Mauß F, Moréac G, Zeuch T. A comprehensive and compact n-heptane oxidation model derived using chemical lumping. Phys Chem Chem Phys. 2007;9:1107–26. https://doi.org/10.1039/B614712G.

92. Dagaut P, Lecomte F, Mieritz J, Glarborg P. Experimental and kinetic modeling study of the effect of NO and SO_2 on the oxidation of CO-H_2 mixtures. Int J Chem Kinet. 2003;35(11):564–75. https://doi.org/10.1002/kin.10154.

93. Wu KT, Lee HT, Juch CI, Wan HP, Shim HS, Adams BR, Chen SL. Study of syngas co-firing and reburning in a coal fired boiler. Fuel. 2004;83(14–15):1991–2000. https://doi.org/10.1016/j.fuel.2004.03.015.

94. Ranzi E, Sogaro A, Gaffuri P, Pennati G, Faravelli T. A wide range modeling study of methane oxidation. Combust Sci Technol. 1994;96(4–6):279–325. https://doi.org/10.1080/00102209408935359.

95. Nist best fit. 2006. http://kinetics.nist.gov/index.php. Accessed 15 Nov 2019.

96. Tsang W, Hampson RF. Chemical kinetic data base for combustion chemistry. Part I. Methane and related compounds. J Phys Chem Ref Data. 1986;15(3):1087–279. https://doi.org/10.1063/1.555759.

97. Timonen RS, Ratajczak E, Gutman D. The addition and dissociation reaction atomic hydrogen + carbon monoxide. dblharw. oxomethyl. 2. Experimental studies and comparison with theory. J Phys Chem. 1987;91:5325. https://doi.org/10.1021/j100304a037.

98. Jachimowski CJ. Chemical kinetic reaction mechanism for the combustion of propane. Combust Flame. 1984;55(2):213–24. https://doi.org/10.1016/0010-2180(84)90029-4.

99. Gardiner WCJ, editor. Combustion chemistry. New York: Springer; 1984. https://doi.org/10.1007/978-1-4684-0186-8.

100. Michael JV, Su MC, Sutherland JW, Carroll JJ, Wagner AF. Rate constants for H + O2 + M f HO2 + M in seven Bath gases. J Phys Chem A. 2002;106:5297–313. https://doi.org/10.1021/jp020229w.

101. Westbrook CK, Dryer F. Chemical kinetic modeling of hydrocarbon combustion. Prog Energy Combust Sci. 1984;10(1):1–57. https://doi.org/10.1016/0360-1285(84)90118-7.

102. Peeters J, Mahnew G. Reaction mechanisms and rate constants ofelementary steps in methane-oxygen flames. Symp Combust. 1973;1973(14):133–46. https://doi.org/10.1016/S0082-0784(73)80015-3.

103. Petersen EL, Davidson DF, Hanson RK. Kinetics modeling of shock-induced ignition in low-dilution CH4/O2 mixtures at high pressures and intermediate temperatures. Combust Flame. 1999;117:272–90. https://doi.org/10.1016/S0010-2180(98)00111-4.

104. Goodings JM, Hayhurst ANJ. Heat release and radical recombination in premixed fuel-lean flames of H2+ O2+ N2. Rate constants for H + OH + M → H2O + M and HO2+ OH → H2O + O2. Chem Soc Faraday Trans 2. 1988;84:745–62. https://doi.org/10.1039/F29888400745.

105. Hong Z, Vasu SS, Davidson DF, Hanson RK. Experimental study of the rate of OH + HO2 f H2O + O2 at high temperatures using the reverse reaction. J Phys Chem A. 2010;114:5520–5. https://doi.org/10.1021/jp100739t.

106. Wooldridge MS, Hanson RK, Bowman CT. A shock tube study of CO + OH → CO2 + H and HNCO + OH → products via simultaneous laser absorption measurements of OH and CO_2. Int J

Chem Kinet. 1996;28:361–72. https://doi.org/10.1002/(SICI)1097-4601(1996)28:5<361::AID-KIN5>3.0.CO;2-T.

107. Zhao Z, Li J, Kazakov A, Dryer FL. Temperature-dependent feature sensitivity analysis for combustion modeling. Int J Chem Kinet. 2005;37:282. https://doi.org/10.1002/kin.20080.

108. Joshi AV, Wang H. Master equation modeling of wide range temperature and pressure dependence of CO + OH → products. Int J Chem Kinet. 2006;38:57. https://doi.org/10.1002/kin.20137.

109. Wooldridge MS, Hanson RK, Bowman CT. A shock tube study of the CO+OH → CO2 +H reaction. Proc Combust Inst. 1994;25:741–8. https://doi.org/10.1016/S0082-0784(06)80706-X.

110. Golden DM, Smith GP, McEwen AB, Yu CL, Eitneer B, Frenklach M, Vaghjiani GL, Ravishankara AR, Tully FP. OH (OD) + CO: measurements and an optimized RRKM fit. J Phys Chem A. 1998;102(44):8598–606. https://doi.org/10.1021/jp982110m.

111. Sun HY, Yang SI, Jomaas G, Law CK. High-pressure laminar flame speeds and kinetic modeling of carbon monoxide/hydrogen combustion. Proc Combust Inst. 2006;31(1):439–46. https://doi.org/10.1016/j.proci.2006.07.193.

112. Lin MC, Bauer SH. Bimolecular reaction of N2O with CO and the recombination of O and CO as studied in a single-pulse shock tube. J Chem Phys. 1969;50:3377. https://doi.org/10.1063/1.1671561.

113. Warnatz J. Rate coefficients in the C/H/O system. In: Gardiner Jr WC, editor. Combustion chemistry. New York: Springer; 1984. p. 197–360. https://doi.org/10.1007/978-1-4684-0186-8.

114. Hardy JW, Gardiner WC Jr, Burcat A. Recombination of carbon monoxide and oxygen atoms. Int J Chem Kinet. 1974;10:503–17. https://doi.org/10.1002/kin.550100508.

115. Wagner HG, Zabel F, Bunsenges B. Neuere Untersuchungen zum thermischen Zerfall von CO2. Teil II. Phys Chem. 1974;72:705. https://doi.org/10.1002/bbpc.19740780717.

116. Inn ECY. Rate of recombination of oxygen atoms and CO at temperatures below ambient. J Chem Phys. 1974;61:1589. https://doi.org/10.1063/1.1682139.

117. Simonaitis R, Heicklen J. Kinetics and mechanism of the reaction of O (3P) with carbon monoxide. J Chem Phys. 1972;56:2004. https://doi.org/10.1063/1.1677490.

118. Toby S, Sheth S, Toby FS. The chemistry of combustion processes. In: Sloane TM, editor. ACS symposium series, vol. 249. Washington: DC pp; 1984. p. 267–76. https://doi.org/10.1021/bk-1983-0249.ch016.

119. Kondratiev VN. On the rate of CO + O recombination. React Kinet Catal Lett. 1974;1:7–13. https://doi.org/10.1007/BF02075114.

120. Kondratiev VN. Proc Combust Inst. 1959;7:41.

121. Allen MT, Yetter RA, Dryer FL. High pressure studies of moist carbon monoxide/nitrous oxide kinetics. Combust Flame. 1997;109:449–70. https://doi.org/10.1016/S0010-2180(96)00181-2.

122. Troe J. Thermal dissociation and recombination of polyatomic molecules. Proc Combust Inst. 1975;15(1):667–80. https://doi.org/10.1016/S0082-0784(75)80337-7.

123. Faravelli T, Frassoldati A, Ranzi E. Kinetic modeling of the interactions between NO and hydrocarbons in the oxidation of hydrocarbons at low temperatures. Combust Flame. 132:188–207. https://doi.org/10.1016/S0010-2180(02)00437-6.

124. Frassoldati A, Faravelli T, Ranzi E. Kinetic modeling of the interactions between NO and hydrocarbons at high temperature. Combust Flame. 2003;135:97–112. https://doi.org/10.1016/S0010-2180(03)00152-4.

125. Boivin P, Jiménez C, Sánchez AL, Williams FA. A four-step reduced mechanism for syngas combustion. Combust Flame. 2011;158(6):1059–63. https://doi.org/10.1016/j.combustflame.2010.10.023.

126. Boivin P, Jiménez C, Sánchez AL, Williams FA. An explicit reduced mechanism for H2–air combustion. Proc Combust Inst. 2011;33(1):517–23. https://doi.org/10.1016/j.proci.2010.05.002.

127. Burke MP, Chaos M, Dryer FL, Ju Y. Negative pressure dependence of mass burning rates of H2/CO/O2/diluent flames at low flame temperatures. Combust Flame. 2010;157(4):618–31. https://doi.org/10.1016/j.combustflame.2009.08.009.

128. Burke MP, Chen Z, Ju Y, Dryer FL. Effect of cylindrical confinement on the determination of laminar flame speeds using outwardly propagating flames. Combust Flame. 2009;156(4):771–9. https://doi.org/10.1016/j.combustflame.2009.01.013.

129. Delattin F, Di Lorenzo G, Rizzo S, Bram S, De Ruyck J. Combustion of syngas in a pressurized microturbine-like combustor: experimental results. Appl Energy. 2010;87(4):1441–52. https://doi.org/10.1016/j.apenergy.2009.08.046.